Molecular Therapy
Original Article

The Chemokine Receptors Ccr5 and Cxcr6 Enhance Migration of Mesenchymal Stem Cells into the Degenerating Retina

Martina Pesaresi,[1] Sergi A. Bonilla-Pons,[1,2] Ruben Sebastian-Perez,[1] Umberto Di Vicino,[1] Marc Alcoverro-Bertran,[1] Ralph Michael,[3,4] and Maria Pia Cosma[1,5,6,7]

[1]Center for Genomic Regulation (CRG), Barcelona Institute of Science and Technology, Dr. Aiguader 88, Barcelona 08003, Spain; [2]Universitat de Barcelona (UB), Barcelona 08028, Spain; [3]Institut Universitari Barraquer, Universitat Autónoma de Barcelona, Barcelona 08021, Spain; [4]Centro de Oftalmología Barraquer, Barcelona 08021, Spain; [5]Universitat Pompeu Fabra (UPF), Barcelona 08003, Spain; [6]ICREA, Passeig de Lluis Companys 23, Barcelona 08010, Spain; [7]Bioland Laboratory (Guangzhou Regenerative Medicine and Health Guangdong Laboratory), Guangzhou 510005, China

Cell therapy approaches hold great potential for treating retinopathies, which are currently incurable. This study addresses the problem of inadequate migration and integration of transplanted cells into the host retina. To this end, we have identified the chemokines that were most upregulated during retinal degeneration and that could chemoattract mesenchymal stem cells (MSCs). The results were observed using a pharmacological model of ganglion/amacrine cell degeneration and a genetic model of retinitis pigmentosa, from both mice and human retinae. Remarkably, MSCs overexpressing Ccr5 and Cxcr6, which are receptors bound by a subset of the identified chemokines, displayed improved migration after transplantation in the degenerating retina. They also led to enhanced rescue of cell death and to preservation of electrophysiological function. Overall, we show that chemokines released from the degenerating retinae can drive migration of transplanted stem cells, and that overexpression of chemokine receptors can improve cell therapy-based regenerative approaches.

INTRODUCTION

Retinopathies are currently incurable. They inevitably lead to visual disabilities and, in most cases, blindness. Worryingly, the number of people affected by retinopathies is estimated to increase dramatically during the next few decades, due both to growth and aging of the population.[1]

Stem cell therapy (SCT) has been proposed as a potential solution to the incurability of degenerative retinal conditions. Therapeutically, stem cells (SCs) transplanted into the eye can exert beneficial effects in one of two ways. First, they can release biologically active molecules. This paracrine effect has potent neuroprotective and anti-inflammatory properties; it strongly promotes the survival, proliferation, and self-repair of endogenous cells.[2] Second, SCs can generate new tissue-specific cells, thereby replacing lost or damaged ones. To facilitate this process, SCs can be differentiated toward specific desired progenitor types *in vitro*, prior to transplantation.[3,4] Although promising.[5–14] SCTs require further development and optimization. In particular, cells transplanted into the eye do not efficiently migrate and integrate into the retina,[3,6,15–17] especially following intravitreal injection.[18,19] In the present study, we address the problem of inadequate migration and integration of transplanted cells.

We used mesenchymal SCs (MSCs) derived from the bone marrow of mice, as their paracrine activity has been extensively characterized.[2,20] The plethora of cytokines and neurotrophic factors they secrete are critical for the repair of injured tissues and deceleration of disease progression.[21–32] Additionally, MSCs display a broad differentiation potential. Indeed, given the appropriate environmental conditions, MSCs can be converted into a variety of neural cell types, including photoreceptors.[33–35] Furthermore, MSCs can be easily expanded *ex vivo*, which provides for abundant starting material for transplantation.[36] Prolonged *ex vivo* expansion is currently not possible for other cell sources such as hematopoietic SCs.[37]

To study chemokine-mediated migration of MSCs we used two distinct degeneration models. First, we used a pharmacological model, *N*-methyl-D-aspartate (NMDA)-induced excitotoxicity. NMDA induces acute loss of ganglion and amacrine neurons.[38–41] In parallel, we used the *rd10* mouse model of autosomal recessive retinitis pigmentosa (RP). The *rd10* mouse carries a missense point mutation in exon 13 of the rod-specific β subunit of the guanosine 3′,5′-cyclic monophosphate (cGMP)-phosphodiesterase (*Pde6b*) gene.[42,43] Pde6b is involved in the phototransduction cascade, and its absence induces progressive loss of both rod and cone photoreceptors. The peak of retinal inflammation in response to cellular damage and

Received 3 June 2020; accepted 23 October 2020;
https://doi.org/10.1016/j.ymthe.2020.10.026.

Correspondence: Maria Pia Cosma, Center for Genomic Regulation (CRG), Barcelona Institute of Science and Technology, Dr. Aiguader 88, Barcelona 08003, Spain.
E-mail: pia.cosma@crg.es

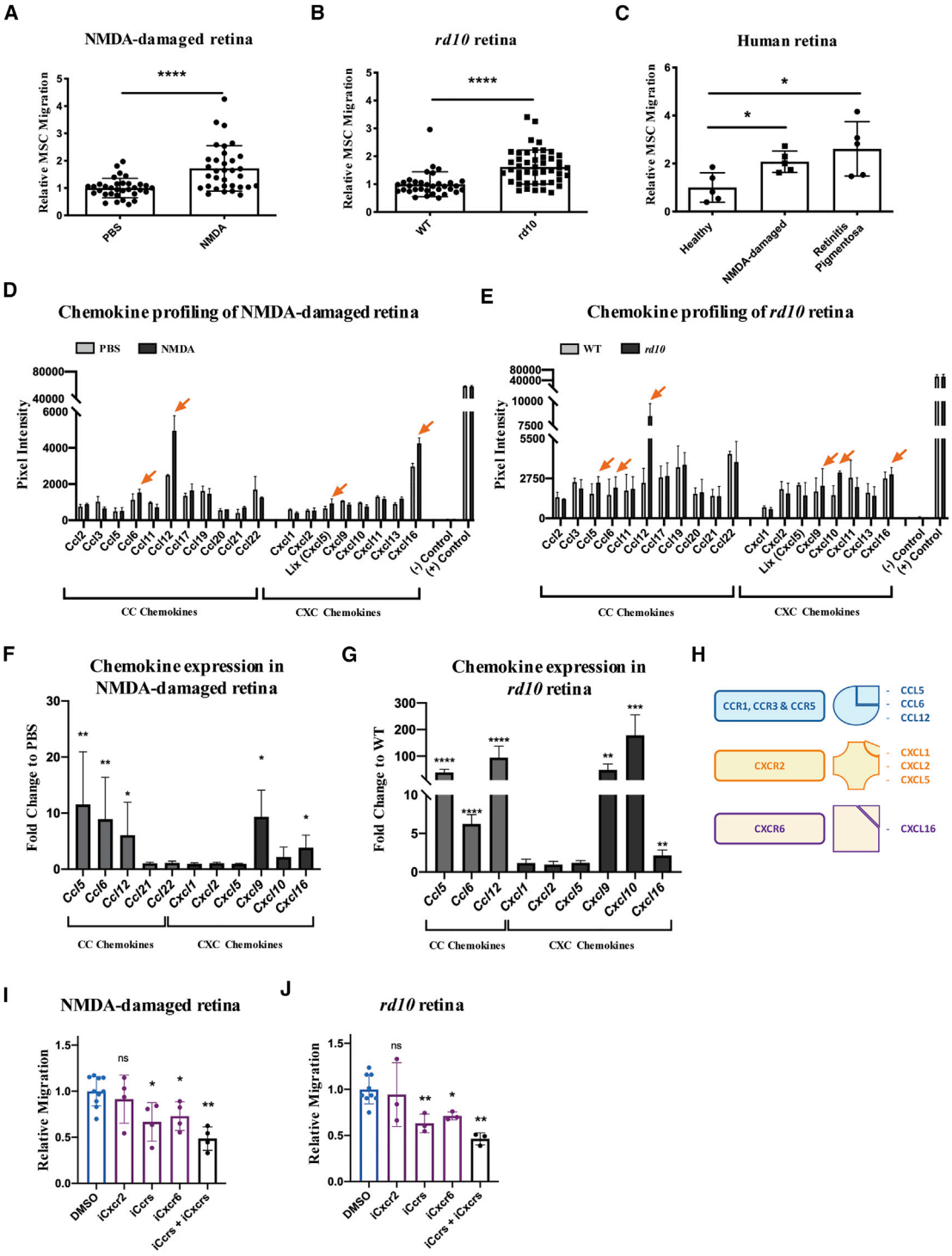

Figure 1. Ccr1, Ccr3, Ccr5, and Cxcr6 Mediate Chemoattraction of MSCs toward Media Conditioned by Degenerating Retinae

(A and B) Quantification of migrated MSCs toward the conditioned media from either (A) PBS- versus NMDA-injected eyecups or (B) WT versus *rd10* P18 eyecups. Number of migrated cells is expressed as fold change relative to control samples (PBS-injected or WT). Data are presented as mean ± SD ($n \geq 3$). A Mann-Whitney test was used for statistical analysis. (C) Quantification of migrated MSCs toward the conditioned media from human retinae cultured in control medium, NMDA-containing medium, or from RP-affected retinae. The number of migrated cells is expressed as fold change relative to control retinae. Data are presented as mean ± SD ($n \geq 3$). (D and E) A Mann-Whitney test was used for statistical analysis. CC and CXC inflammatory chemokine profiles from either (D) PBS- versus NMDA-injected retinae (24 h post-infection [hpi]) or (E) WT

(legend continued on next page)

photoreceptor loss occurs at postnatal day 18 (P18).[42,44] Additionally, we performed experiments using human retinae isolated from deceased donors and cultured *ex vivo*. We compared retinae cultured under control conditions either to retinae exposed to NMDA or to retinae of deceased patients affected by RP.

We identified damage-dependent chemokines that are secreted by the degenerating retina and demonstrated that these chemokines function as chemoattractants for MSCs. We showed that expression of Ccr5 and Cxcr6 significantly improved migration of MSCs *ex vivo* and *in vivo*. This ameliorated neuronal death and improved the electrophysiology response. In conclusion, this study shows that genetic manipulation of MSCs can significantly advance efforts to optimize cell therapy-based regenerative approaches.

RESULTS

Damage-Dependent Soluble Factors Chemoattract MSCs

Tissue injury induces the release of chemotactic factors.[45,46] For this reason, we hypothesized the peak of the acute injury response to be concomitant with the maximum secretion of soluble molecules able to chemoattract MSCs. In order to identify such a peak, we analyzed expression of interleukin-1β (*Il1-β*) at multiple time points following NMDA injection (Figure S1A), and at various postnatal days in *rd10* mice (Figure S1B). In accordance with previously published studies,[42,44] we found that *Il1-β* expression peaked 24 h after NMDA injection, and at P18 in the *rd10* mouse, eventually reaching low levels 1 month after NMDA damage, and at 6 months of age (adult) for the *rd10* mice (Figures S1A and S1B).

We then performed transwell-based chemotactic assays using mouse eyecups 24 h after NMDA injection and at P18 for the *rd10* mouse (Figure S1C). We found that media conditioned by degenerating retinae stimulated migration of MSCs to a greater extent than media from control samples (Figures 1A and 1B; Figures S1D and S1E). Given the high structural and functional similarity that exists among injury-dependent molecules in mice and humans,[46] we also decided to perform chemotactic experiments using conditioned media from cultured human retinae (Figure S1G). We found that MSCs migrated more efficiently both toward NMDA-damaged retinae and toward retinae from patients with RP (Figure 1C; Figure S1F). In conclusion, our results indicate that upon retinal damage soluble factors are secreted and they can chemoattract MSCs.

Chemotactic Pathways That Elicit Migration of MSCs

We next profiled the inflammatory chemokines present in murine retinal lysates, prepared at 24 h after NMDA injection and at P18 for the *rd10* mouse. We decided to focus on the two largest and most extensively characterized families of chemokines, i.e., the CC and the CXC.[46] Compared to their control counterparts, degenerating retinae showed heightened levels of multiple inflammatory chemokines (Figures 1D and 1E). Most notably, levels of Ccl6, Ccl12, and Cxcl16 were increased in both models. In contrast, Cxcl5 was increased only in NMDA-damaged retinae, and Ccl5, Cxcl9, and Cxcl10 were increased only in the *rd10* retina. Results from the cytokine arrays were validated by gene expression analysis, performed at multiple time points following NMDA injections and postnatal days in the *rd10* mice (Figures S2A and S2D). We found that chemokine expression followed a trend that was predictably similar to that of *Il1-β* (Figures S2B, S2C, S2E, and S2F). We confirmed a strong, damage-dependent upregulation of *Ccl5*, *Ccl6*, *Ccl12*, *Cxcl9*, *Cxcl10*, and *Cxcl16*, 24 h after NMDA injection and at P18 for the *rd10* mouse (Figures 1F and 1G).

We also investigated gene expression changes in human retinae isolated from deceased donors and cultured *ex vivo* (Figures S2G and S2H). We could detect injury responses both in retinae exposed to NMDA and in retinae from patients with RP, as indicated by the upregulation of *Il1-β* and tumor necrosis factor alpha (*TNF-α*) (Figure S2G). Upregulation of *Il1-β* and *TNF-α* was accompanied by increased expression of multiple CC and CXC chemokines, including *CCL5*, *CCL22*, *CCL23* (*mCcl6*), *CXCL3* (*mCxcl1*), *CXCL10*, *CXCL11* and *CXCL16* (Figure S2H).

Based on the expression data from degenerating retinae, we identified various CC and CXC ligand-receptor axes that could potentially be involved in the recruitment of migratory cells. These included Ccl5/6/12-Ccr1/Ccr3/Ccr5, Cxcl9/10-Cxcr3, and Cxcl16-Cxcr6 (Figure 1H). We also further investigated the Cxcl1/2/5-Cxcr2 axis, as it was known to recruit MSCs in other degenerative contexts.[47,48] Therefore, we performed transwell assays in the presence of small-molecule antagonists of chemokine receptors (Figures 1I and 1J; Figure S2I). In particular, we used inhibitors of the Ccr1, Ccr3, and Ccr5 receptors, a Cxcr2 inhibitor, and a Cxcr6 inhibitor. Of note, we opted for combined inhibition of the three Ccr receptors, as they can all be bound by Ccl5. In the context of both NMDA-induced (Figure 1I) and RP-induced (Figure 1J) degenerations, we found that migration of MSCs could be significantly reduced either by inhibition of the Cxcr6 receptor, or by combined inhibition of Ccr1, Ccr3, and Ccr5.

versus *rd10* P18 retinal lysates. Pixel intensity is directly proportional to the total amount of protein in the sample. Orange arrows point to representative chemokines whose abundance is increased in degenerating retinae (NMDA or *rd10*), relative to controls (PBS or WT). Data are presented as mean ± SD from n = 2 independent experiments. (F and G) qRT-PCR of CC and CXC inflammatory chemokines from (F) NMDA-damaged (24 hpi) and (G) *rd10* (P18) retinae. Transcript levels are expressed as fold change relative to control (PBS-injected or WT) retinae. Data are presented as mean ± SD ($n \geq 3$). A Mann-Whitney test was used for statistical analysis. (H) Scheme summarizing the interactions among chemokine receptors and ligands of interest. Ccr1, Ccr3, and Ccr5 are bound by Ccl5, Ccl6, and Ccl12. Cxcr2 is bound by Cxcl1, Cxcl2, and Cxcl5. Cxcr6 is bound by Cxcl16. (I and J) Quantification of migrated MSCs toward the conditioned media from either (I) NMDA-damaged (24 hpi) or (J) *rd10* (P18) retinae, in the presence of the inhibitors of Ccrs (Ccr1, Ccr3, and Ccr5 [iCcrs]), Cxcr2 (iCxcr2), Cxcr6 (iCxcr6) or Ccrs + Cxcrs (Ccr1, Ccr3, Ccr5 [iCcrs]; Cxcr2 and Cxcr6 [iCxcrs]). Number of migrated cells is expressed as fold change to control (vehicle, DMSO). Data are presented as minimum (Min) to maximum (Max) boxes (with line at median) from $n \geq 3$ independent experiments. A Mann-Whitney test was used for statistical analysis.

However, the chemotactic response of MSCs was not affected by the inhibition of Cxcr2. The combined inhibition of Ccr and Cxcr receptors led to an even stronger reduction in MSC migration. In conclusion, our results indicate that Ccr1, Ccr3, Ccr5, and Cxcr6 activation can elicit migration of MSCs in the context of retina degeneration.

Generating and Characterizing MSCs That Overexpress Specific CC and CXC Chemokine Receptors

Next, we profiled the endogenous expression levels of Ccr1, Ccr3, Ccr5, Cxcr2, Cxcr3, and Cxcr6 in MSCs. In accordance with published literature,[48,49] we found that MSCs expressed chemokine receptors at an almost negligible level when compared to the mesenchymal marker Thy (Figure S3A). Thus, we generated six distinct overexpressing (OE-)MSC lines, one for each of the aforementioned receptors. Generating OE-MSCs was achieved via lentiviral infection of constructs containing both the hemagglutinin (HA)-tagged receptor and an EGFP reporter (*EF1α_HA-receptor*-SV40_*EGFP*; Figure S3B). The resulting OE-MSC lines were characterized using multiple approaches. First, we ensured that receptor mRNAs were upregulated (Figure S3C). Second, we used immunofluorescence to confirm the expression of the GFP marker and HA-tag (Figure S3D). Third, we used fluorescence-activated cell sorting (FACS) to check for the presence of the receptors at the cell surface (Figure 2A). Finally, we determined that the receptors were functional. To this end, we performed transwell assays to assess the migration of wild-type (WT)- and OE-MSCs toward chemically-defined chemokine gradients (Figure 2B). We tested the following receptor-chemokine pairs: Ccr1/Ccr3/Ccr5-Ccl5, Cxcr2-Cxcl1, Cxcr3-Cxcl10, and Cxcr16-Cxcl6. In all cases, we found that OE-MSCs migrated significantly more than did their WT counterparts (Figure 2B). This indicated that the exogenously expressed receptors can respond to chemokine gradients established by their cognate ligands. Collectively, our results showed that OE-MSCs expressed relatively high levels of the transduced chemokine receptors, and that such receptors were functional and correctly localized at the cell surface.

OE-MSCs Display Enhanced Migration

Next, we tested migration of OE-MSCs in transwell assays using media conditioned by degenerating retinae. The results showed that overexpression of Ccr1, Ccr5, Cxcr2, or Cxcr6 could significantly increase the migration of MSCs toward the media conditioned by both NMDA-damaged (Figure 2C) and *rd10* retinae (Figure 2D).

Based on these results, we tested the migration of OE-MSC lines overexpressing Ccr5, Cxcr2, or Cxcr6 in chemotactic assays with media conditioned by both NMDA-damaged and RP-affected human retinae. We opted for Ccr5 rather than Ccr1 because most MSCs endogenously express Ccr1 (Figure 2A). MSCs from all three overexpressing lines migrated more extensively than did WT-MSCs in both degenerative models (Figures 2E and 2F).

We therefore proceeded to test migration of Ccr5, Cxcr2, and Cxcr6 OE-MSCs *in vivo*. MSCs were transplanted intravitreally at 12 h after NMDA injection. After 4 days from transplantation (4 days post-injection [4 dpi]), animals were sacrificed, and the percentage of MSCs in the retina was quantified by flow cytometry (Figure 2G). Our results showed that overexpression of either Ccr5 or Cxcr6, but not Cxcr2, led to a significant increase in the percentage of GFP^+ MSCs in the retina (Figure 2H; Figures S3F and S3G).

Combined Overexpression of Ccr5 and Cxcr6 Further Enhances Migration of MSCs

Since transplanted OE-MSCs overexpressing either Ccr5 or Cxcr6 showed significantly increased migration *in vivo*, we tested whether combined overexpression of the two receptors would lead to a further improvement in cell migration. To do so, we generated a double overexpressing (dOE) MSC line. This was achieved via simultaneous infection of MSCs with two lentiviral constructs, each one driving expression of a single receptor (Figure S4A). First, we ensured that dOE-MSCs were overexpressing both Ccr5 and Cxcr6 (Figures S4B and S4C). Of note, mRNA levels of Ccr5 and Cxcr6 in dOE-MSCs were found to be comparable to that of single expressing OE-MSC lines (i.e., Ccr5-MSC and Cxcr6-MSC). Second, we confirmed by immunofluorescence that the cells expressed the GFP and the HA tags (Figure S4D). Third, we performed flow cytometry to ensure that the phenotype of GFP- and dOE-MSCs had not been altered due to lentiviral infection. We found that WT-, GFP-, and dOE-MSCs expressed the same SC surface markers. They were positive for the mesenchymal markers CD44, CD90, and Sca-I and negative for CD45, CD34, and CD11b[50] (Figure S4E). Additionally, since chemokine signaling can be involved in the regulation of cell proliferation, we confirmed that GFP- and dOE-MSCs showed comparable expression of *cyclin D1* (Figure S4F), which is a marker of proliferative cells.[51] We also analyzed the expression of multiple factors that are known to mediate the neuroprotective paracrine effects of MSCs in the retina,[21,52,53] including brain-derived neurotrophic factor (*Bdnf*), nerve growth factor (*Ngf*), platelet-derived growth factor alpha (*Pdgf-α*), and ciliary neurotrophic factor (*Ctnf*). We did not observe any statistically significant difference in the expression of such neurotrophic factors between GFP- and dOE-MSCs (Figures S4G and S4J). We further showed that the secretory profiles were comparable by analyzing the media conditioned by either GFP- or dOE-MSCs. We found that there were no significant changes in the secretion of EGF, FGF-1, PDGF, PIGF-2, and VEGF (Figure S4K). Lastly, we performed chemotactic assays toward a chemically defined gradient of Ccl5 and Cxcl16 to ensure that exogenously expressed Ccr5 and Cxcr6 were functional (Figure S4L). We then tested the migration of dOE-MSCs toward medium conditioned by degenerating retinae. We found that MSCs expressing both chemokine receptors migrated better than WT and MSCs expressing either receptor alone (Figures 3A and 3B). Finally, we tested the *in vivo* migration of dOE cells by FACS analysis after transplantation. This showed that the number of GFP^+ cells in the retinae was highest for MSCs expressing both Ccr5 and Cxcr6 (Figure 3C; Figure S4M).

To investigate the long-term migration and integration, we transplanted either WT- or dOE-MSCs into NMDA-damaged retinae following intravitreal transplantation and P18 *rd10* retinae following

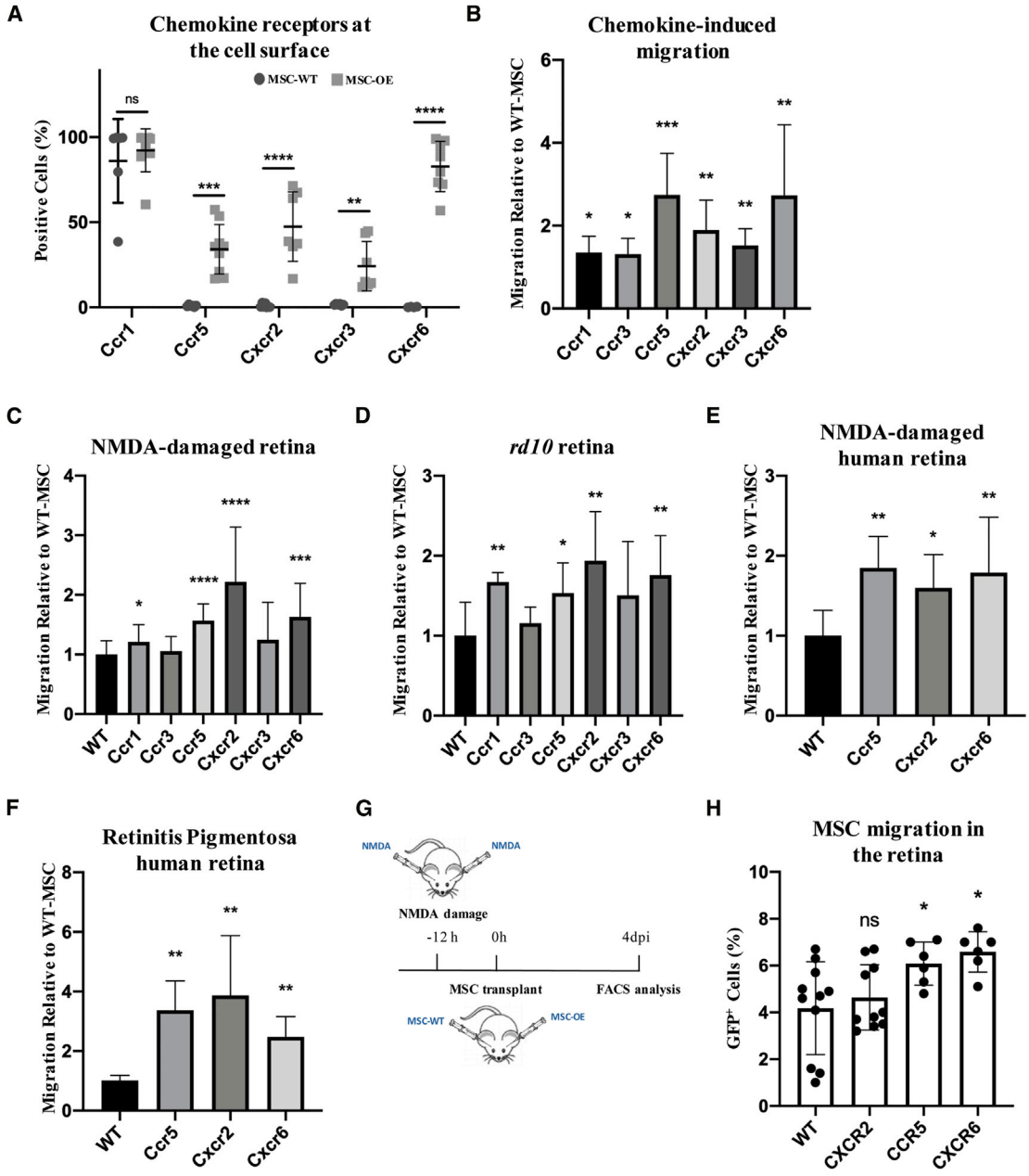

Figure 2. OE-MSCs Display an Increased Chemotactic Response Toward the Media Conditioned by Damaged Retinae and Improved Migration following Transplantation in the Vitreous

(A) Cell-surface FACS analysis of Ccr1, Ccr5, Cxcr2, Cxcr3, and Cxcr6 receptors of the corresponding OE-MSC lines, and of WT-MSCs as a control. Results are expressed as the percentage of positive cells. Data are presented as mean ± SD from n ≥ 3 independent experiments. A two-tailed Student's t test was used for statistical analysis. (B) Quantification of migrated MSCs toward a concentration of 50 ng/mL of Ccl5 (Ccr1-MSC, Ccr3-MSC, and Ccr5-MSC), Cxcl1 (Cxcr2-MSC), Cxcl10 (Cxcr3-MSC), or Cxcl16 (Cxcr6-MSC) from transwell-based assays. The number of migrated cells is expressed as fold change to control (WT-MSCs). Data are presented as mean ± SD from n ≥ 3 independent experiments. A Mann-Whitney test was used for statistical analysis. (C and D) Quantification of migrated MSCs overexpressing the chemokine receptors toward the conditioned media from either (C) NMDA-injected or (D) *rd10* retinae in transwell-based assays. The number of migrated cells (OE-MSCs) is expressed as fold change to control (WT-MSCs). Data are presented as mean ± SD from n ≥ 3 independent experiments. A Mann-Whitney test was used for statistical analysis. (E and F) Quantification of migrated MSCs toward the conditioned media from either (E) NMDA-damaged or (F) RP human retinae in transwell-based assays. Number of migrated cells is expressed as fold change to control (WT-MSCs). Data are presented as mean ± SD from n ≥ 3 independent experiments. A Mann-Whitney test was used for statistical analysis. (G) Experimental scheme. Eyes were damaged via NMDA injection 12 h prior to transplantation of either WT-MSCs or OE-MSCs (Cxcr2-MSCs, Ccr5-MSCs, or Cxcr6-MSCs). FACS analysis was performed 4 days after the transplant (4 dpi). (H) FACS-based quantification of GFP^+ MSCs (WT, Cxcr2, Ccr5, or Cxcr6) in transplanted retinae 4 dpi. Results are expressed as percentage of total retinal cells. Data are presented as Min to Max boxes (with line at median) from n ≥ 3 independent experiments. A two-tailed Student's t test was used for statistical analysis.

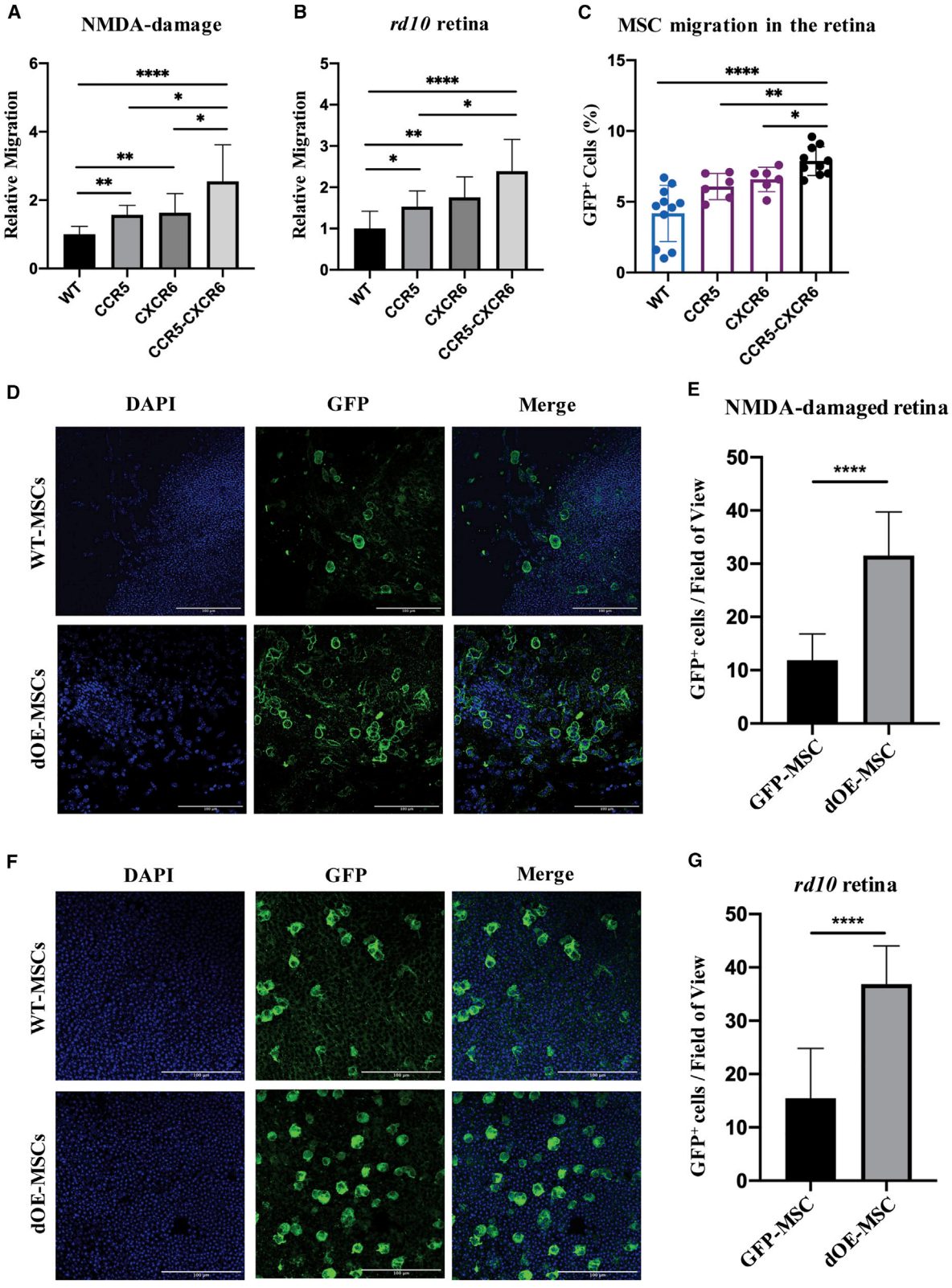

(legend on next page)

subretinal transplantation. We sacrificed the animals 3 weeks after transplantation and counted the number of GFP^+ MSCs in retinal flat mounts (Figures 3D–3G). We found that, compared to the WT controls, the number of dOE-MSCs was 2.7- and 2.4-fold higher in NMDA-damaged and *rd10* retinae, respectively (Figures 3E and 3G). Interestingly, we did not observe the presence of GFP^+ cells in areas that were not visibly damaged by the NMDA, as evidenced by a high number of βIII-tubulin$^+$ cells (Figure S5A), suggesting that MSCs are selectively attracted to the area of damage.

To exclude the possibility that the observed GFP^+ cells were retinal cells that had phagocytosed apoptotic MSCs, we performed an *in vitro* assay to investigate the dynamics of GFP degradation following phagocytosis by retinal pigmented epithelial (RPE) cells (Figures S5B–S5D). We found that RPE cells could phagocytose and rapidly clear apoptotic bodies derived from GFP-MSCs. RPE cells transiently became GFP-positive, with a peak 1–3 h from the exposure to the apoptotic bodies. Within 24 h, most RPE cells had already degraded the internalized GFP and appeared to be GFP-negative. After 72 h, the entire RPE cell population was negative for GFP expression (Figures S5B–S5D). These results suggested that the GFP coming from apoptotic MSCs would be rapidly cleared by phagocytic cells of the retina immediately after transplantation. Thus, it is very unlikely that the GFP^+ cells we observed in the tissue 3 weeks post-injection (wpi) are phagocytic retinal cells. To further support these observations, we also transplanted GFP-MSCs and dOE-MSCs intravitreally in NMDA-damaged transgenic mice ubiquitously expressing DsRed. In this model, all retinal cells are positive for DsRed. Therefore, if a $DsRed^+$ retinal cell phagocytosed a GFP^+ MSC, then the two fluorescent markers would co-localize. Alternatively, the co-localization of the two markers might be the result of cell fusion. Indeed, it has been shown that retinal cells can fuse with transplanted bone marrow-derived SCs.[10,11] We found that at 3 wpi, fewer than 30% of the GFP^+ cells were $DsRed^+$ (Figures S5E–S5G). This might indicate that transplanted MSCs had undergone apoptosis and that apoptotic bodies had been phagocytosed by retinal cells shortly before the mice were sacrificed. Alternatively, and more likely, cell fusion might have occurred; indeed, we found that some GFP^+-$DsRed^+$ cells contained two separated nuclei (Figure S5G). Importantly, either way, more than 70% of the GFP^+ cells were DsRed-negative in the long-term (Figure S5E). In addition, there was no significant difference in the $DsRed^+$-GFP^+/GFP^+ ratio between GFP- and dOE-MSCs ($DsRed^+$-$GFP^+/GFP^+_{GFP\text{-}MSC}$ = 27.2%; $DsRed^+$-$GFP^+/GFP^+_{dOE\text{-}MSC}$ = 29.6%). In conclusion, even though we cannot exclude the possibility of short-term phagocytosis events or cell fusion for a percentage of the transplanted cells, our results suggest that ~70% of the GFP-expressing cells observed in the long term are indeed derived from the transplanted MSCs.

Transplanted Ccr5-Cxcr6 MSCs Rescue Retinal Degeneration

MSCs can rescue tissue degeneration through their paracrine activity.[2,20–22] To investigate the potential beneficial effects of dOE-MSC transplantation, we counted the number of rows of photoreceptor nuclei in sections from *rd10* mice that had received an injection of PBS in one eye, and transplantation of either WT- or dOE-MSCs in the other one (Figures 4A and 4B). We found that retinal sections from control (PBS-injected) eyes contained an average of 1.5 rows, which is indicative of severe photoreceptor degeneration. The number of rows was slightly increased following transplantation of MSCs. However, the outer nuclear layer (ONL) was significantly thicker when dOE-MSCs, rather than WT cells, had been transplanted (Figures 4A and 4B).

We also recorded scotopic electroretinography (ERG) responses from dark-adapted *rd10* animals. Each animal had one eye treated with either WT- or dOE-MSCs; the other eye was used as an internal (PBS-injected) control. We found that the mice could be segregated into two groups. Animals in the first group (n_{WT} = 5, n_{OE} = 5, n_{WT+OE} = 10) showed very small ERG amplitudes. In contrast, animals in the second group (n_{WT} = 3, n_{OE} = 4, n_{WT+OE} = 9) had more prominent ERG amplitudes. We hypothesize that these differences may be due to slower progression of the photoreceptor degeneration in the latter group. For both groups, we calculated the differences in A-wave and B-wave amplitudes (Δ_A, Δ_B) between control (PBS-injected) and experimental (WT/dOE-MSC-injected) eyes. We found that, compared to controls, eyes transplanted with MSCs expressing Ccr5 and Cxcr6 displayed a modest but significant increase in both A- and B-wave amplitudes (Figure 4C).

Transplanted MSCs Express Retinal-Specific Markers in the Long Term

Even though they have been predominantly studied for their paracrine activity, MSCs possess a degree of plasticity that allows their conversion into a variety of cell types, including neuronal cells.[54,55] In order to assess whether MSCs could change their phenotype after transplantation, we stained retinal flat mounts from NMDA-treated animals for βIII-tubulin, a neuron-specific marker expressed by ganglion cells and retinal interneurons.[56] We found that most of the GFP^+ MSCs were positive for βIII-tubulin and appeared integrated in the ganglion cell layer (GCL) (Figures 4D–4F; Figure S6A). βIII-

Figure 3. Overexpression of Ccr5 and Cxcr6 Improves Migration and *In Vivo* Integration of Transplanted MSCs

(A and B) Quantification of migrated MSCs (Ccr5, Cxcr6, or Ccr5-Cxcr6) toward the conditioned media from either (A) NMDA-injected or (B) *rd10* retinae from transwell-based assays. The number of migrated cells is expressed as fold change to control (WT-MSCs). Data are presented as mean ± SD ($n \geq 3$). Mann-Whitney test was used for statistical analysis. (C) FACS-based quantification of GFP^+ MSCs (WT, Ccr5, Cxcr6, or Ccr5-Cxcr6) in transplanted retinae 4 dpi. Results are expressed as percentage of total retinal cells. Data are presented as mean ± SD ($n \geq 3$). A two-tailed Student's t test was used for statistical analysis. (D and F) Representative fields from WT-MSC versus dOE-MSC flat mounts, prepared from either (D) NMDA-injected or (F) *rd10* retinae, and stained against GFP. Scale bars, 100 μm. Either the GCL/INL (D) or the ONL (F) were imaged. (E and G) Quantification of GFP^+ cells counted in at least three fields per animal, in both (E) NMDA-injected and (G) *rd10* retinae ($n \geq 3$). Data are presented as mean ± SD. A two-tailed Student's t test was used for statistical analysis.

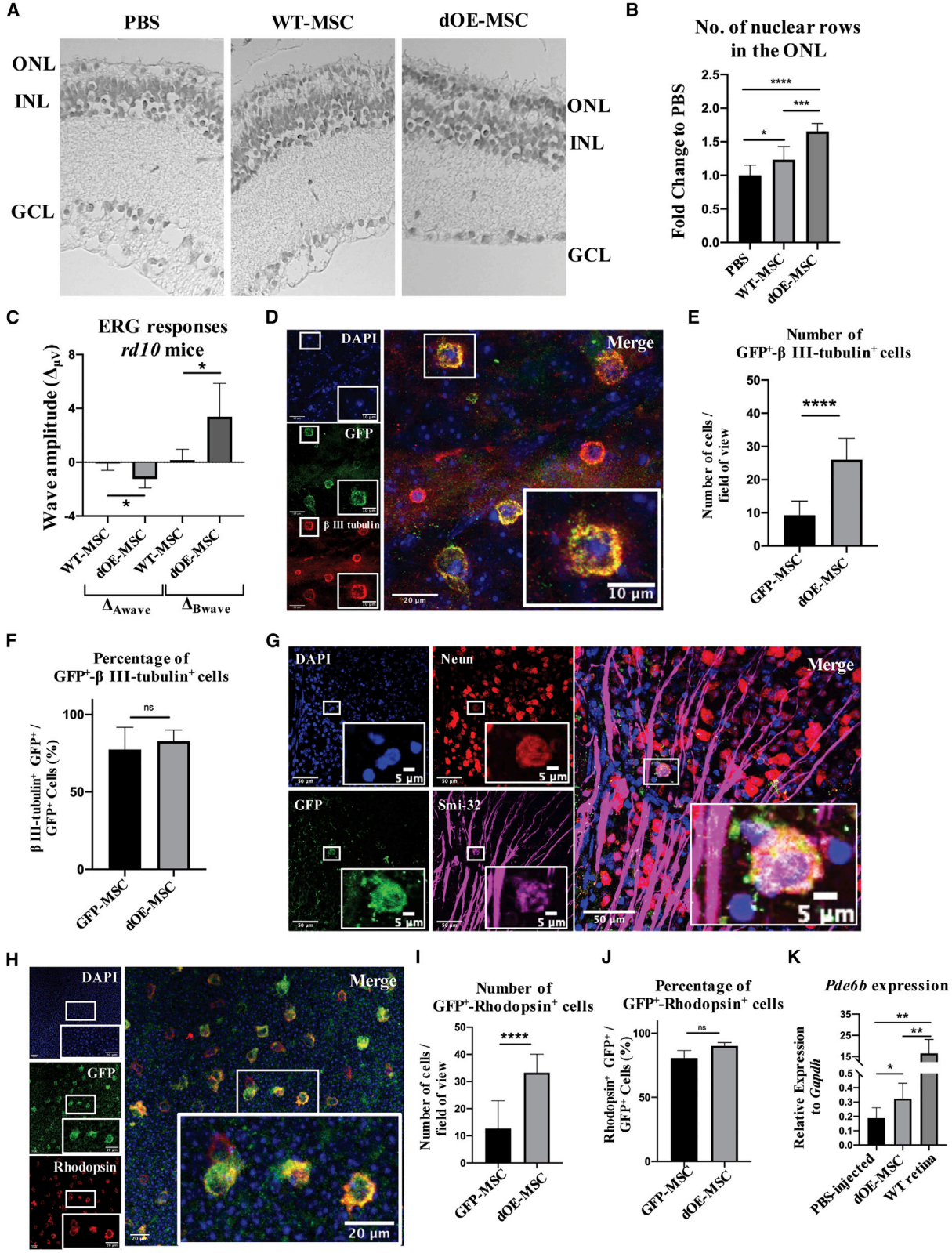

(legend on next page)

tubulin is exclusively expressed in neurons within the CNS. Nonetheless, there is some evidence that it might also be expressed by other cell types (e.g., fibroblasts, keratinocytes, and various cancer cell lines) during metaphase and anaphase.[57] In this direction, we stained retinal flat mounts for βIII-tubulin and phosphorylated (phospho-)histone H3 (Ser10), a marker of mitotic cells.[58] GFP^+ cells were positive for βIII-tubulin but negative for phospho-histone H3 (Figure S6B), suggesting that they could indeed acquire expression of neuronal-specific markers in the long term. To further support this hypothesis, we also stained retinal flat mounts and retinal sections for additional neuronal markers. We found that at 3 wpi, some of the GFP^+ MSCs expressed Neun, Smi-32, and calbindin (Figure 4G; Figures S6C and S6D). Importantly, we found that at 3 wpi, MSCs had lost expression of the mesenchymal marker CD90 (Thy) (Figure S6E). Moreover, MSCs were largely negative for glial marker GFAP expression (Figure S6F), with only 18.7% of the GFP-MSCs and 21.4% of the dOE-MSCs expressing GFAP at 3 wpi (Figure S6G).

Similarly, in the *rd10* retinae, MSCs lost expression of CD90 (Thy) (Figure S7A). Most of the transplanted GFP^+ MSCs were positive for the photoreceptor-specific markers rhodopsin (Figures 4H–4J; Figure S7C) and recoverin (Figure S7D). Moreover, the transplanted MSCs were apparently located within the same layer as $rhodopsin^+$ photoreceptors (Figure S7B), although they did not fully integrate in the ONL, likely due to their large size. Compared to controls, the total number of $GFP^+/βIII\text{-}tubulin^+$ and of $GFP^+/rhodopsin^+$ dOE-MSCs was significantly increased (Figures 4E and 4I). Interestingly, however, we found that the proportion of cells that were positive for βIII-tubulin or rhodopsin was comparable for WT- and dOE-MSCs (Figures 4F and 4J). This indicates that while the number of transplanted MSCs that migrate into the retina is dependent on the expression of Ccr5 and Cxcr6, both WT- and dOE-MSCs, once integrated into the retina, can express retinal-specific markers. We also performed RT-PCR analysis of *rd10* retinae at 3 wpi. We found that transplanting dOE-MSCs could partially restore expression of the *Pde6b* gene (Figure 4K), further suggesting that partially integrated MSCs in the ONL can express genes characteristic of photoreceptors.

In conclusion, upon combined exogenous expression of Ccr5 and Cxcr6, transplanted MSCs can more efficiently migrate toward the host retinae. In accordance with published literature,[21–32] they can then delay the death of neighboring cells, most likely through their potent survival-promoting paracrine activity. At the same time, they can also acquire expression of genes characteristic of ganglion neurons and photoreceptors, highlighting the potential role that cell transdifferentiation could play in delaying retinal degeneration.

DISCUSSION

In this work, we profiled the CC and CXC inflammatory chemokines upregulated in two distinct models of retinal degeneration. We then engineered SCs that displayed improved migration toward media conditioned by degenerating retinae from both mice and humans. *In vivo*, these cells could be efficiently chemoattracted and up to a certain extent integrated into host retinae, thanks to the engagement of the Ccr5 and the Cxcr6 receptors by a subset of the identified CC and CXC chemokines. Importantly, transplantation of Ccr5-Cxcr6-MSCs resulted in a thicker ONL, which was indicative of a rescue of the endogenous photoreceptor cells in a model of RP.

MSC transplantation appears to ameliorate the degenerative phenotype via two distinct mechanisms. First, there is extensive evidence showing that transplanted MSCs mainly promote the survival of endogenous cells through their paracrine and neuroprotective activity.[7,59–63] The neurotrophic factors secreted by MSCs can reduce inflammation, apoptosis, and fibrosis while enhancing neuronal survival and differentiation.[64] There is also evidence that the neuroprotective and anti-inflammatory properties of MSCs are largely mediated by extracellular vesicles (EVs).[64,65] MSC-derived EVs have been shown to reduce cell death and prevent apoptosis in numerous

Figure 4. Functional Rescue of the Retinal Degeneration upon Transplantation of dOE-MSCs

(A) Representative H&E staining of 2-month-old rd10 retinae that had been transplanted with PBS (left), WT-MSCs (center), or dOE-MSCs (right), 3 weeks post-injection (wpi). GCL, ganglion cell layer; INL, inner nuclear layer; ONL, outer nuclear layer. (B) Quantification of photoreceptor rows in retinae that had been transplanted with PBS, WT-MSCs, or dOE-MSCs, 3 wpi. Results are presented as fold change to control (PBS). Data are expressed as mean ± SD (n = 3). A Mann-Whitney test was used for statistical analysis. (C) Statistical analysis of ERG responses of 2-month-old rd10 mice that had received transplantation of MSCs (either WT or dOE) in one eye, and of vehicle alone (PBS) in the other eye, 3 wpi. Data are presented as mean ± SD (n = 2) of the difference between the amplitudes of the waves recoded in the MSC-injected eye and of those recorded in the contralateral (PBS-injected) eye ($\Delta_{\mu V}$). A two-tailed Student's t test was used for statistical analysis. (D) Representative field of view from a retinal flat mount prepared from an NMDA-damaged eye at 3 wpi that had been transplanted with dOE-MSCs. The tissue was stained for GFP (green), βIII-tubulin (red), and DAPI (blue). Scale bars, 20 μm. Inserts at the bottom-right corner show higher magnification of the regions in the white square (scale bars, 10 μm). (E and F) Quantification of GFP^+-$βIII\text{-}tubulin^+$ double-positive cells from retinal flat mounts, expressed either as number of cells per field of view (E), or as percentage of GFP^+-$βIII\text{-}tubulin^+$ cells over the total GFP^+ cells in the field of view (F). Data are presented as mean ± SD (n = 3). A two-tailed Student's t test was used for statistical analysis. (G) Representative field of view from a retinal flat mount prepared from an NMDA-damaged eye at 3 wpi that had been transplanted with dOE-MSCs. The tissue was stained for GFP (green), Neun (red), Smi-32 (magenta), and DAPI (blue). Scale bars, 50 μm. Inserts at the bottom-right corner show higher magnification of the regions in the white square (scale bars, 5 μm). (H) Representative field of view from a retinal flat mount prepared at 3 wpi from an rd10 eye that had been transplanted with dOE-MSCs. The tissue was stained for GFP (green), rhodopsin (red), and DAPI (blue). Scale bars, 20 μm. Inserts at the bottom-right corner show higher magnification of the regions in the white square (scale bars, 20 μm). (I and J) Quantification of GFP^+-$rhodopsin^+$ double-positive cells from retinal flat mounts, expressed either as number of cells per field of view (I), or as percentage of GFP^+-$rhodopsin^+$ cells over the total GFP^+ cells in the field of view (J). Data are presented as mean ± SD (n = 3). A two-tailed Student's t test was used for statistical analysis. (K) RT-PCR of Pde6b expression in retinae harvested from rd10 retinae that had been transplanted at P18 either with PBS or dOE-MSCs. Data are presented as mean ± SD (n = 3). A two-tailed Student's t test was used for statistical analysis.

disease models, including bone and cartilage degeneration,[66,67] neurological disorders,[68–72] liver injury,[73–75] kidney failure,[76,77] muscle degeneration,[78,79] and cardiovascular diseases.[80,81] Intravitreal administration of MSC-derived EVs has been shown to enhance functional recovery while decreasing neuro-inflammation and apoptosis in models of retinal ischemia,[82] glaucoma,[83] and autoimmune uveitis.[84] Interestingly, the protection conferred by EVs seems to be higher when multiple administrations are performed[83] or when EVs are injected in high doses.[84] In this direction, transplant of dOE-MSCs with an improved migratory capability could result in an enhanced rescue of the degenerative phenotype, due to the constant release of EVs close to the injury site.

Alternatively, it is noteworthy that in the medium-to-long term, MSCs lose expression of the mesenchymal marker CD90 (Thy), while acquiring expression of retina-specific neuronal and glial markers. These results suggest the possibility that transplanted MSCs might potentially convert into functional retinal cell types and replace lost cells. Nonetheless, we have not investigated these transdifferentiation events in detail. Further evidence and single-cell studies are required to determine whether MSCs can differentiate into mature retinal cells. Electrophysiological responses measured at the level of individual cells might give useful insights in the future. Likewise, the membrane potentials characteristic of neurons, or their response to neurotransmitters, could be investigated. Additional studies are also needed with respect to cell integration. In fact, our results showed that intravitreally transplanted MSCs could reach the GCL and integrate within the tissue. However, subretinally transplanted MSCs could not properly integrate within the photoreceptor nuclear layers, most likely due to their large size. Cultured MSCs are more than 20 μm in diameter, which might limit or impede their penetration through the outer limiting membrane and inside the layer of tightly compacted photoreceptors.[85] Therapeutic approaches specifically aiming at cell replacement in the ONL might be more successful if photoreceptor precursor cells expressing Ccr5 and Cxcr6 were used. Strategies facilitating the penetration through the outer limiting membrane would probably further enhance the results. On the basis of these considerations, we hypothesize the paracrine activity of transplanted MSCs to be mostly responsible for the ameliorated degenerative phenotype.

Strategies similar to the one we propose have already been used in different disease contexts, including epidermolysis bullosa,[47] radiation-induced oral mucositis,[48] and myocardium infarct.[86] Importantly, the chemotactic axis exploited in these studies varied. For instance, Cxcr2-MSCs performed better than WT-MSCs in the context of epidermolysis bullosa and radiation-induced oral mucositis.[47,48] However, in the infarcted myocardium, Cxcr2-MSCs did not migrate better than their WT counterparts, while Ccr1-MSCs did.[86] In our study, we identified and characterized the Ccr5 and the Cxcr6 receptors. We found that only a small percentage of the total MSC population expresses either Ccr5 (<1%) or Cxcr6 (<0.5%) on their surface. Our results are consistent with published literature,[48,49] and they highlight the limited repertoire of chemokine receptors that MSCs endogenously express. It is also important to consider that the MSC chemokine receptor profile is sensitive to time in culture.[87] More specifically, prolonged *ex vivo* cell culturing and expansion might lead to substantial downregulation of chemokine receptor expression.[87] Genetic modification of cultured MSCs would allow overcoming such a problem.

In the past, CC and CXC chemokines have been shown to synergize to increase leukocyte recruitment to inflamed tissues.[88] The specific mechanisms regulating such synergy have not been clearly elucidated yet. However, it has been suggested that synergistic effects could result from receptor heterodimerization[89] or chemokine cooperation at the level of intracellular signal transduction.[90] Either way, synergistic interactions between chemokines that are concomitantly released can contribute to the enhancement and the fine-tuning of inflammatory responses. We took advantage of the existence of such cooperative mechanism to boost the recruitment of exogenously transplanted MSCs via combined expression of Ccr5 and Cxcr6.

Notably, the subsets of upregulated chemokines were strikingly similar and largely overlapping in our two degenerative models. Indeed, a strong increase in Ccl5, Ccl6, Ccl12, and Cxcl16 was also reported in other disease models, including autoimmune uveitis and age-related macular degeneration (AMD).[91–97] This is not particularly surprising, as inflammatory responses of the retina are mainly orchestrated by Müller glial cells (MGCs), RPE cells, and activated microglia, independent of the cell type that is initially damaged.[98] For instance, Ccl5 in the P18 *rd10* mouse retina is produced by microglial cells and MGCs of the inner nuclear layer (INL).[99] Crucially, the existence of these highly comparable, site-specific (rather than disease-specific) patterns of chemokine upregulation would make our strategy widely applicable, and suitable even for patients with other types of retinopathies, such as AMD or optic neuropathies.

A recent study reported that homogenates from injured brains play a repulsive role on MSC migration.[100] In this study, we used conditioned media rather than tissue homogenates for *ex vivo* transwell assays. By doing so, we have specifically investigated migration of MSCs toward the soluble factors released by the damaged retina, which, *in vivo*, are responsible for chemoattraction. When tissue homogenates are used instead, intracellular factors are also released and might alter the overall results of the experiments. Of note, the ischemic brain environment also appears to inhibit MSC migration into the parenchyma *in vivo*.[100] When intra-arterially administered, MSCs are kept in the perivascular niche, from where they can exert their therapeutic actions, including the release of EVs and neurotrophic factors. These are intriguing observations that appear to disagree with our results. Nonetheless, the local microenvironment of the injured retina might differ significantly from that of the ischemic brain. Additionally, we administered MSCs locally rather than systemically. In other words, MSCs are not in direct contact with the microenvironment established by the vessel walls, which might effectively retain them, preventing their extravasation.

Survival and integration of transplanted cells can be tremendously affected by the administration route used. Systemic administration

by intravenous injection is commonly used for MSCs, as it is safe and allows for the infusion of a large amount of cells. However, it generally shows low efficiency with respect to homing to the injury site, as MSCs get trapped in the lungs and cleared.[101–104] Additionally, even if they could escape lung entrapment, their migration into the retina would be further prevented by the blood-retinal barrier. This could explain why systemically transplanted MSCs can be short-lived[104] and why they generally fail to reach the retina and to exert neuroprotective effects.[9] In contrast, direct delivery into tissues can allow MSCs to escape systemic clearance and to persist locally up to several weeks.[105] As a consequence, in the context of retinal disease, MSCs are preferably administered via either intravitreal or subretinal injections. In our study, locally transplanted MSCs could survive at least 3 weeks. Of note, the suitability of each administration route may vary depending on the type and on the extent of tissue damage. As a general rule, intravitreal injection is preferred when ganglions and/or INL neuronal cells are damaged, whereas subretinal administration is the standard route in the context of photoreceptor loss.

Our strategy could have an extremely high degree of adaptability and versatility, as it could potentially be applied to any type of transplanted cells. As a significant example, it could be used to improve homing of retinal and/or photoreceptor precursors cells, which are inherently good at differentiating into mature retinal neurons, but display very poor migratory capabilities.[106–109] The success of our approach is dependent on the secretion of chemotactic factors into the vitreous cavity. Importantly, this is known to happen during retinal degeneration in human patients.[110–113] Indeed, there seems to be a correlation between the number of inflammatory cells recruited in the vitreous cavity and the visual function of the patient: the higher the former, the lower the latter.[114] For instance, CXCL16 levels in the aqueous humor of wet AMD patients positively correlate with lesion size.[113] Importantly, in human RP patients, inflammation is chronic. Even though stronger inflammatory reactions are generally found in younger patients with active disease processes, the inflammatory state continues even after photoreceptor loss.[114] Such persistent inflammation means that the levels of chemokines released by the tissue will be elevated throughout the patient's lifespan. This is consistent with our results, which showed that conditioned medium from the retina of elderly RP patients can strongly chemoattract MSCs. In fact, the samples we received were all from patients who passed away at an age of at least 65, and therefore had already gone through the acute phase of photoreceptor loss.

Despite the promising results presented in this study, our strategy holds potential for further improvement. In particular, OE-MSC lines were generated via lentiviral infection. In a clinical setting, this would raise important concerns with respect to the risk of tumorigenesis. In fact, lentiviral vectors randomly integrate into the genome and can therefore lead to harmful mutations. A number of potentially valid alternatives to lentiviral infection are available, including Sendai viruses or adenoviral vectors. Alternatively, non-viral systems (e.g., naked DNA or synthetic mRNAs) could be used.[115] The identification of safer and less-invasive delivery strategies, coupled to the establishment of detailed procedures for the generation of clinical-grade cells, will undoubtedly help overcome some of the major hurdles that currently hinder the translation of SCT approaches to the clinical setting.

In conclusion, this study provides a viable approach to the challenge of achieving effective delivery and engraftment at the site of injury, and it shows that genetic manipulation of SCs prior to transplantation can significantly aid the further development of cell therapy-based regenerative approaches. Undoubtedly, there is still considerable work to be carried out. Nonetheless, our findings could eventually be integrated with complementary optimization strategies to make SCT in the eye a feasible and realistic option for treating retinopathies, and for achieving visual restoration.

MATERIALS AND METHODS

Cell and Tissue Culture

Primary MSCs derived from the bone-marrow of mice (C57BL/6) were purchased from Gibco (S1502-100). They were produced from the bone marrow isolated from C57BL/6 mice at $\leq$8 weeks of gestation through mechanical and enzymatic digestion and were maintained in DMEM/F-12-GlutaMAX supplemented with 10% fetal bovine serum (FBS), penicillin (100 U/mL), and streptomycin (100 μg/mL). For all experiments, MSCs were used between passage 10 and 16. Human RPE cells were purchased from ATCC (CRL-2302) and maintained in DMEM/F-12-GlutaMAX supplemented with 10% FBS, penicillin (100 U/mL), and streptomycin (100 μg/mL). Mouse eyecups were prepared by removing the cornea, the iris, and the vitreous and then cultured in serum-free (SF) DMEM/F-12-GlutaMAX with penicillin (100 U/mL) and streptomycin (100 μg/mL). Human retinae were dissected and cultured in SF Neurobasal-A medium supplemented with GlutaMAX (0.5%), N2 (1×), B27 (1×), penicillin (100 U/mL), and streptomycin (100 μg/mL).

Animal Care and Treatment

Mice were maintained under a 12-h light/12-h dark cycle with access to food and water *ad libitum*, in accordance with the Ethical Committee for Animal Experimentation (CEEA) of the Government of Catalonia. The CEEA of the Parc de Recerca Biomèdica de Barcelona (PRBB, Spain) reviewed and approved all animal procedures. Additionally, procedures and experiments were performed in accordance with the ARVO (The Association for Research in Vision and Ophthalmology) Statement for the Use of Animals in Ophthalmic and Vision Research, and with ARRIVE (Animal Research: Reporting of *In Vivo* Experiments) guidelines.[116] Male and female C57BL/6 mice between 8 and 12 weeks of age were used for the experiments involving transplantation following NMDA damage; *rd10* (and corresponding WT control) C57BL/6 mice were transplanted at P18 and sacrificed at endpoints detailed in each of the experiments. We also used the CAG-DsRed transgenic mouse line, obtained from The Jackson Laboratory (stock no. 006051).[117] In all experiments, animals were assigned randomly to the various treatment groups. At least three mice per treatment group were used. General anesthesia was induced when needed with intraperitoneal injection of ketamine

(70 mg/kg) and medetomidine (10 mg/kg). Anesthesia was reversed with atipamezole (2 mg/kg). At endpoints, mice were euthanized using CO_2.

Retinal Damage and Cell Transplantation

Mice were anaesthetized and intravitreally injected with 2 μL of either NMDA (20 mmol/μL; Sigma) or PBS, as a control. Briefly, a 30G needle was used to carefully make a small, punch incision at the upper temporal ora serrata. The 33G needle of a Hamilton's syringe was then inserted into the incision, angled toward the optic nerve, to inject PBS or NMDA into the vitreous. The needle was left in place for a couple of seconds before being retracted to avoid reflux of the injected solutions.

For cell transplantation, MSCs were detached using Accutase (StemPro Accutase cell dissociation reagent, Life Technologies), counted, and resuspended in PBS plus chondroitinase ABC (ChABC, 0.1 U/μL) at a concentration of 150,000 cells/μL. Adult mice that had received NMDA damage were transplanted intravitreally with 2 μL of MSCs (i.e., 300,000 cells) 12 h post-injection.[117] P18 *rd10* mice were transplanted subretinally with 1 μL of MSCs (i.e., 150,000 cells), as previously described.

Human Retina Culture

The research adhered to the tenets of the Declaration of Helsinki on research involving human subjects. The experimental protocol was approved by the Ethical Committee for Clinical Research of the Centro de Oftalmología Barraquer. Human donor eyes were obtained from the "Banc d'Ulls per a Tractaments de Ceguesa." Written informed consent for the removal and use of the eyes for diagnostic and research purposes was obtained from donors and/or relatives. All of the samples we received were from donors aged 65–90.

The retinae were dissected using a procedure and a setup optimized in our laboratory in collaboration with the Centro de Oftalmología Barraquer. Briefly, the cornea, iris, crystalline, and vitreal excess were removed. The retina was then separated from the RPE and from the rest of the eye. After the removal of the periphery and of the vitreal leftovers, the central part of the retina was cultured for 12 h and then processed for experiments.

RNA Extraction and Quantitative Real-Time PCR

RNA was extracted and purified using an RNA isolation mini kit (-QIAGEN), according to the manufacturer's protocol. Total RNA was treated with DNase I (QIAGEN) to prevent DNA contamination. The cDNA was produced with SuperScript III reverse transcriptase kits (Invitrogen). Quantitative real-time PCR reactions were prepared using Platinum SYBR Green qPCix-UDG (Invitrogen) and run in a LyghtCycler 480 (Roche) machine, according to the manufacturer's recommendations. Quantitative real-time PCR analysis was performed in technical duplicates, for a minimum of three biological replicates (with the exception of human retinae with RP, where n = 2). Quantitative real-time PCR data were normalized to GAPDH expression. The oligonucleotides used are listed in Table S1.

For the investigation of NMDA damage, eye samples were collected 24 h (24 hpi), 48 h (48 hpi), 4 days (4 dpi), 7 days (7 dpi), or 4 weeks (4 wpi) post-injection. *Rd10* mice were sacrificed at P14, P18, P22, and at 6 months of age (adults). To study gene expression in human retinae, RNA was extracted following 24-h culturing in SF medium with or without NMDA (1 mM).

Chemotactic Assays

Chemotactic assays were performed using transwell inserts (pore size, 8 μm, BD Biosciences, 353182) and 12-well culture plates. To test migration toward defined chemokine gradients, lower chambers were loaded with 1.2 mL of SF DMEM/F-12-GlutaMAX medium with either mCcl5, mCxcl1, mCxcl10, mCxcl16, or a combination of Ccl5 and mCxcl16 (all 50 ng/mL, PeproTech). For the NMDA damage, mice were sacrificed 24 hpi; *rd10* mice were sacrificed at P18. Human retinae were dissected and cultured for an initial 12 h in Neurobasal-A medium, as previously described. Afterward, both mouse and human retinae were cultured for 24 h in SF DMEM/F-12-GlutaMAX and SF Neurobasal-A (with or without 1 mM NMDA), respectively. 1.2 mL of the resulting conditioned medium was loaded in the lower chambers of the transwell. The upper chamber was loaded with 2×10^5 MSCs in SF medium. The medium used to resuspend MSCs was matched to the medium in the bottom chamber, that is, either DMEM/F-12-GlutaMAX (to test migration toward medium conditioned by mouse retinae) or Neurobasal-A (to test migration toward medium conditioned by human retinae). To test chemokine receptor inhibition, MSCs were incubated for 20 min at 4°C with small-molecule receptor antagonists (used as indicated in Table S2), prior to being used in chemotactic assays.

Transwell plates were incubated for 1.5 h at 37°C. Afterward, cells remaining on the upper surface of the inserts were removed with a cotton swab. Tranwells were then washed (PBS), fixed (4% paraformaldehyde [PFA], 10 min), and stained with 5 mg/mL 4′,6-diamidino-2-phenylindole (DAPI, Sigma). For each insert, seven fields were imaged and analyzed. Cells were automatically counted using a custom-made macro for ImageJ software (US National Institutes of Health, Bethesda, MD, USA; https://rsb.info.nih.gov/ij/).

Chemokine Antibody Arrays

Proteome Profiler mouse chemokine antibody array (R&D Systems) was used to assay retinal lysates derived from PBS/NMDA-injected mice (24 hpi) and from WT/*rd10* mice (P18). The manufacturer's recommendations were followed. Briefly, retinae were excised and homogenized in PBS with protease inhibitors (10 μg/mL aprotinin, 10 μg/mL leupeptin, and 10 μg/mL pepstatin). After homogenization, Triton X-100 was added to the sample to a final concentration of 1%. Samples were then frozen at −20°C, thawed, and centrifuged at 10,000 × *g* for 5 min. Arrays were probed with a total of 200 μg of protein. Membranes were developed by standard chemiluminescence techniques. Pixel intensity was quantified using ImageJ software. The net level of each protein was calculated by the mean of the individual spot intensity minus the mean of the background intensity. Relative spot intensities are presented as mean ± SD.

Lentiviral Constructs and MSC Infection

Mouse *Ccr1*, *Ccr3*, *Ccr5*, *Cxcr2*, *Cxcr3*, and *Cxcr6* coding sequences (CDSs) were amplified by reverse transcribing total mouse spleen RNA (SuperScript III RT kit, Invitrogen) and then amplifying the full-length CDSs by PCR (using Phusion hot start high-fidelity polymerase, Thermo Fisher Scientific). The oligonucleotides used are listed in Table S3. Resultant cDNA was C-terminally tagged with HA and inserted into a lentiviral vector with a p1494 backbone, containing an EF1α promoter. An EGFP reporter was also present, with its expression being driven by a constitutive SV40 promoter (*EF1α_HA-receptor*-SV40_*EGFP*). To generate the Ccr5-Cxcr6, double-expressing line of MSCs, the constitutive EGFP reporter of the *EF1α_HA-receptor*-SV40_*EGFP* construct was replaced by a hygromycin resistance marker (*EF1α_HA-Cxcr6*-SV40_*Hygro*).

For infection, lentiviral particles were produced following the RNAi Consortium (TRC) instructions for lentiviral particle production and infection in 10-cm plates (https://www.broadinstitute.org/rnai/public/). At day 0, HEK293 cells were plated at a density of 5×10^4 cells/cm^2 in p150 plates. At day 1, using a calcium phosphate transfection kit (Clontech Laboratories, 631312), cells were co-transfected with (1) 19.5 μg of pCMV-DR8.2, (2) 10.5 μg of pCMV-vesicular stomatitis virus glycoprotein G (VSV-G), or (3) 30 μg of the *EF1α_ HA-receptor*-SV40_*EGFP* or the *EF1α_ HA-Ccr5*-SV40_*EGFP* + *EF1α_ HA-Cxcr6-SV40_Hygro* construct. At day 2, the medium of the transfected HEK293 was replaced with fresh DMEM/F-12-GlutaMAX supplemented with 30% FBS. Meanwhile, MSCs were plated at a density of 5×10^4 cells/cm^2. The lentiviral particle-containing medium was harvested from HEK293T cells at 48 and 72 h post-transfection (days 3 and 4), filtered, and directly used for cell infection.

MSCs infected with *EF1α_ HA-eceptor-SV40_EGFP* constructs were FACS sorted based on fluorescence intensity. Cells transduced with *EF1α_Ccr5-SV40_EGFP* + *EF1α_ HA-Cxcr6-SV40_Hygro* were FACS sorted based on fluorescence intensity and subjected to hygromycin selection (50 μg/mL) starting 2 days after the second round of infection.

Immunofluorescence of Cultured Cells

MSCs were plated into Lab-Tek chambers. The following day, they were washed (PBS), fixed (4% PFA, 10 min), and permeabilized (0.2% Triton X-100 in PBS, 10 min). Non-specific binding of antibodies was blocked by a 1-h incubation with a solution of PBS with 3% BSA, 300 μM glycine, and 0.03% Triton X-100. Incubation with primary antibodies lasted 3 h (at room temperature). Cells were then washed with PBS and incubated with secondary antibodies (1.5 h, at room temperature). DAPI (5 mg/mL) was used to stain nuclei. Images were acquired using a Leica SP8 confocal microscope. The following antibodies were used: chicken anti-GFP (1:200; ab13970, Abcam), mouse anti-HA (1:150; 11583816001, Roche), anti-chicken Alexa Fluor 488, and anti-mouse Alexa Fluor 568. All secondary antibodies were provided by Molecular Probes (Invitrogen) and used at 1:1,000 in PBS.

Profiling of Secreted Factors

Proteome Profiler mouse angiogenesis array (R&D Systems) was used to assay SF DMEM/F-12-GlutaMAX medium that had been conditioned by either GFP-MSCs or dOE-MSCs, cultured for 24 h. Arrays were probed with a total of 800 μg of protein. Membranes were developed by standard chemiluminescence techniques. Pixel intensity was quantified using ImageJ software. The net level of each protein was calculated by the mean of the individual spot intensity minus the mean of the background intensity. Relative spot intensities are presented as mean ± SD.

Flow Cytometry Analysis of MSCs and Retinal Samples

For flow cytometry, cultured MSCs were detached with Accutase and collected by centrifugation at 300 relative centrifugal force (rcf) for 5 min. They were resuspended at a concentration of 1×10^6 cells/mL and incubated with purified rat anti-mouse CD16/CD32 (mouse BD Fc Block; BD Pharmingen) at a concentration of 5 μg/mL (in PBS), 20 min at 4°C, to block non-specific binding of antibodies. Following two washes in PBS, cells were incubated with conjugated primary antibodies (in PBS) for 30 min at 4°C, in the dark. Finally, they were washed (PBS) and resuspended in PBS for flow cytometry. DAPI (5 mg/mL) was added to exclude dead cells. The following antibodies were used: phycoerythrin (PE) anti-mouse CCR1 (FAB5986P; R&D Systems), allophycocyanin (APC) anti-human/mouse/rat CCR5 (FAB1802A; R&D Systems), peridinin chlorophyll protein (PerCP) anti-mouse CXCR2/interleukin-8RB (IL-8RB) (FAB2164C; R&D Systems), Alexa Fluor 700 anti-mouse CXCR3 (FAB1685N; R&D Systems), Alexa Fluor 700 anti-mouse CXCR6 (FAB2145N; R&D Systems), PE anti-mouse CD90.2 (12-0902; eBioscience), PE anti-mouse CD44 (12-0441-82; eBioscience), PE anti-mouse CD34 (551387; BD Biosciences), PE anti-mouse CD45 (553081; BD Biosciences), PE-Cy7 anti-mouse Ly-6A/E (Sca-I) (25-5981; eBioscience), and PE-Cy7 anti-mouse CD11b (552850; BD Biosciences). All antibodies were used at a concentration of 10 μL/10^6 cells.

For flow cytometry analysis of retinal samples, retinae were dissected from the enucleated eyes and incubated (30 min, 37°C) in trypsin supplemented with 0.1 mg/mL DNase I for 20–30 minutes at 37°C. Samples were then mechanically triturated, filtered, pelleted, and re-suspended in PBS. DAPI (5 mg/mL) was added to exclude dead cells. Both NMDA-damaged *rd10* eyes were analyzed at 4 dpi. All data were processed and analyzed with FlowJo (v10).

Fixing, Sectioning, and Immunofluorescence

Eyes were enucleated and fixed by immersion in 4% PFA overnight at 4°C; they were embedded in paraffin the following day. 5-μm-thick sections oriented orthogonally to the retinal layers were prepared and processed for either immunofluorescence or hematoxylin and eosin staining. Briefly, for the immunofluorescence, sections were deparaffinized by sequential treatment with xylene and EtOH gradient; slices were then placed in a plastic rack with a permeabilization buffer containing 0.3% Triton X-100 and 0.1 M sodium citrate in PBS (1 h at room temperature). Antigen retrieval was then performed by boiling

the slides for 4 min in a domestic microwave. After a wash with cold water, non-specific binding of antibodies was blocked by a 1-h incubation with a solution of PBS with 3% BSA, 300 μM glycine, and 0.03% Triton X-100. Sections were then incubated with primary antibodies diluted in PBS, 1.5% BSA (twice overnight at 4°C). On the following day, slides were washed with PBS and incubated with secondary antibodies for 2 h at room temperature.

For retinal flat mount immunostaining, whole retinae were dissected from previously fixed eye globes, and left an additional 30 min in 4% PFA. They were then permeabilized (0.3% Triton X-100 in PBS, 1.5 h at room temperature). Non-specific binding of antibodies was blocked by a 1-h incubation with a solution of PBS with 3% BSA, 300 μM glycine, and 0.03% Triton X-100. Incubation with primary antibodies lasted 48 h at 4°C. Retinae were then washed with PBS and incubated with secondary antibodies (24 h at 4°C). DAPI (5 mg/mL) was also used to stain for cell nuclei.

The following primary antibodies were used: chicken anti-GFP (1:200; ab13970, Abcam), mouse anti-βIII-tubulin (1:200; ab7751, Abcam), mouse anti-Smi-32 (1:200; 5598440001, Merck), mouse anti-calbindin (1:200; C7354, Sigma), mouse anti-GFAP (1:200; MAB360, Millipore), rabbit anti-Neun (1:200; ab177487, Abcam), mouse anti-rhodopsin (1:200; MAB5356, Millipore), rabbit anti-recoverin (1:200; AB5585, Merck Life Science), rabbit anti-phosphohistone-H3 (Ser10) (1:200; 06-570, Millipore), and rat anti-CD90.2 (1:150; 14-0902-82, eBioscience). The following secondary antibodies were used: anti-chicken Alexa Fluor 488, anti-mouse Alexa Fluor 568, anti-mouse Alexa Fluor 647, anti-rabbit Alexa Fluor 568, and anti-rat Alexa Fluor 568. All secondary antibodies were used at 1:1,000 in PBS. DAPI (5 mg/mL) was used to stain for cell nuclei.

Both retinal flat mounts and sections were mounted with Vectashield (Vector Laboratories, Burlingame, CA, USA) and imaged using either Leica laser SP5 or SP8 confocal microscopy systems.

Images from both sections and whole retinal flat mounts were processed with the ImageJ software. Cell counts were based on analysis of at least three animals. For each section and flat mount, we imaged a minimum of three fields.

Apoptotic Assay

For the apoptotic assays, GFP-MSCs were seeded at a density of 7.5×10^3 cells/cm^2. After 24 h of culturing, they were treated with 5 μM doxorubicin for an additional 24 h to induce apoptosis. The apoptotic bodies released in the medium were collected by centrifugation at 300 rcf for 7 min. They were then resuspended in fresh DMEM/F-12-GlutaMAX medium and seeded on top of human RPE cells, seeded at a density of 2×10^4 cells/cm^2 24 h prior to the assay. RPE cells and GFP-MSC-derived apoptotic bodies were co-cultured for 1, 3, 6, 12, 24, 48, or 72 h. At the moment of the analysis, cells were trypsinized, collected, and resuspended in PBS. Flow cytometry analysis was performed with an LSRFortessa analyzer (BD Biosciences). All flow cytometry data were processed and analyzed with FlowJo (v10).

Statistical Analysis

As specified in the figure legends, data are presented as mean ± SD. All statistical tests and graphs were generated using the Prism 8.0 software (GraphPad, San Diego, CA. USA). Depending on the experimental setup, we used a Mann-Whitney test, two-tailed Student's t test, or one-way ANOVA. In all cases, a p value <0.05 was considered significant (*$p < 0.05$, **$p < 0.01$, ***$p < 0.001$, ****$p < 0.0001$; ns, not significant). In experiments where internal reference samples were used to normalize data across different replicates, their expression was set to 1. To show the internal variability of these reference samples, we calculated their SD relative to their internal average value.

SUPPLEMENTAL INFORMATION

Supplemental Information can be found online at https://doi.org/10.1016/j.ymthe.2020.10.026.

AUTHOR CONTRIBUTIONS

M.P. and M.P.C. conceived and designed the study. M.P., S.A.B.-P., R.S.-P., U.D.V., and M.A.-B. performed experiments. R.M. provided help with the human retinae experiments. M.P. analyzed data. M.P. and M.P.C. wrote the manuscript. M.P.C. supervised the project.

CONFLICTS OF INTEREST

The authors declare no competing interests.

ACKNOWLEDGMENTS

We thank Prof. Peter F. Hitchcock for his precious and critical suggestions on the content and style of the manuscript. We also thank the UPF/CRG Flow Cytometry Unit, the CRG Advanced Light Microscopy Unit, and the PRBB animal facility (PRBB, Barcelona). Finally, we thank Alberto Oliveri for help with the graphical abstract. This work was supported by Velux Stiftung (976a to M.P.C.); La Caixa Health (HR17-00231); the Ministerio de Ciencia e Innovacion (BFU2017-86760-P to M.P.C.) (AEI/FEDER, UE); the AGAUR grant from the Secretaria d'Universitats i Recerca del Departament d'Empresa i Coneixement de la Generalitat de Catalunya (2017 SGR 689 to M.P.C.); the Subprograma Estatal de Formación del Ministerio de Economía y Competitividad (refs. BES-2015-072802 to M.P. and BES-2015-075805 to S.A.B.-P.); the Secretaria d'Universitats i Recerca del Departament d'Empresa i Coneixement de la Generalitat de Catalunya (ref. 2018FI_B_00637 to R.S.-P.); and by the co-finance of Fondo Social Europeo (FSE to R.S.-P.). We acknowledge support of the Spanish Ministry of Science and Innovation to the EMBL partnership, the Centro de Excelencia Severo Ochoa, and the CERCA Programme/Generalitat de Catalunya.

REFERENCES

1. Bourne, R.R.A., Flaxman, S.R., Braithwaite, T., Cicinelli, M.V., Das, A., Jonas, J.B., Keeffe, J., Kempen, J.H., Leasher, J., Limburg, H., et al.; Vision Loss Expert Group (2017). Magnitude, temporal trends, and projections of the global prevalence of blindness and distance and near vision impairment: a systematic review and meta-analysis. Lancet Glob. Health *5*, e888–e897.

2. Baraniak, P.R., and McDevitt, T.C. (2010). Stem cell paracrine actions and tissue regeneration. Regen. Med. *5*, 121–143.

3. MacLaren, R.E., Pearson, R.A., MacNeil, A., Douglas, R.H., Salt, T.E., Akimoto, M., Swaroop, A., Sowden, J.C., and Ali, R.R. (2006). Retinal repair by transplantation of photoreceptor precursors. Nature *444*, 203–207.

4. Eberle, D., Santos-Ferreira, T., Grahl, S., and Ader, M. (2014). Subretinal transplantation of MACS purified photoreceptor precursor cells into the adult mouse retina. J. Vis. Exp. (84), e50932.

5. Lund, R.D., Wang, S., Lu, B., Girman, S., Holmes, T., Sauvé, Y., Messina, D.J., Harris, I.R., Kihm, A.J., Harmon, A.M., et al. (2007). Cells isolated from umbilical cord tissue rescue photoreceptors and visual functions in a rodent model of retinal disease. Stem Cells *25*, 602–611.

6. Inoue, Y., Iriyama, A., Ueno, S., Takahashi, H., Kondo, M., Tamaki, Y., Araie, M., and Yanagi, Y. (2007). Subretinal transplantation of bone marrow mesenchymal stem cells delays retinal degeneration in the RCS rat model of retinal degeneration. Exp. Eye Res. *85*, 234–241.

7. Tzameret, A., Sher, I., Belkin, M., Treves, A.J., Meir, A., Nagler, A., Levkovitch-Verbin, H., Barshack, I., Rosner, M., and Rotenstreich, Y. (2014). Transplantation of human bone marrow mesenchymal stem cells as a thin subretinal layer ameliorates retinal degeneration in a rat model of retinal dystrophy. Exp. Eye Res. *118*, 135–144.

8. Arnhold, S., Absenger, Y., Klein, H., Addicks, K., and Schraermeyer, U. (2007). Transplantation of bone marrow-derived mesenchymal stem cells rescue photoreceptor cells in the dystrophic retina of the rhodopsin knockout mouse. Graefes Arch. Clin. Exp. Ophthalmol. *245*, 414–422.

9. Johnson, T.V., Bull, N.D., Hunt, D.P., Marina, N., Tomarev, S.I., and Martin, K.R. (2010). Neuroprotective effects of intravitreal mesenchymal stem cell transplantation in experimental glaucoma. Invest. Ophthalmol. Vis. Sci. *51*, 2051–2059.

10. Sanges, D., Simonte, G., Di Vicino, U., Romo, N., Pinilla, I., Nicolás, M., and Cosma, M.P. (2016). Reprogramming Müller glia via in vivo cell fusion regenerates murine photoreceptors. J. Clin. Invest. *126*, 3104–3116.

11. Sanges, D., Romo, N., Simonte, G., Di Vicino, U., Tahoces, A.D., Fernández, E., and Cosma, M.P. (2013). Wnt/β-catenin signaling triggers neuron reprogramming and regeneration in the mouse retina. Cell Rep. *4*, 271–286.

12. Meyer, J.S., Katz, M.L., Maruniak, J.A., and Kirk, M.D. (2006). Embryonic stem cell-derived neural progenitors incorporate into degenerating retina and enhance survival of host photoreceptors. Stem Cells *24*, 274–283.

13. Nishida, A., Takahashi, M., Tanihara, H., Nakano, I., Takahashi, J.B., Mizoguchi, A., Ide, C., and Honda, Y. (2000). Incorporation and differentiation of hippocampus-derived neural stem cells transplanted in injured adult rat retina. Invest. Ophthalmol. Vis. Sci. *41*, 4268–4274.

14. Pearson, R.A., Barber, A.C., Rizzi, M., Hippert, C., Xue, T., West, E.L., Duran, Y., Smith, A.J., Chuang, J.Z., Azam, S.A., et al. (2012). Restoration of vision after transplantation of photoreceptors. Nature *485*, 99–103.

15. Jiang, C., Klassen, H., Zhang, X., and Young, M. (2010). Laser injury promotes migration and integration of retinal progenitor cells into host retina. Mol. Vis. *16*, 983–990.

16. Singh, M.S., Balmer, J., Barnard, A.R., Aslam, S.A., Moralli, D., Green, C.M., Barnea-Cramer, A., Duncan, I., and MacLaren, R.E. (2016). Transplanted photoreceptor precursors transfer proteins to host photoreceptors by a mechanism of cytoplasmic fusion. Nat. Commun. *7*, 13537.

17. Zhou, L., Wang, W., Liu, Y., Fernandez de Castro, J., Ezashi, T., Telugu, B.P., Roberts, R.M., Kaplan, H.J., and Dean, D.C. (2011). Differentiation of induced pluripotent stem cells of swine into rod photoreceptors and their integration into the retina. Stem Cells *29*, 972–980.

18. Johnson, T.V., Bull, N.D., and Martin, K.R. (2009). Transplantation prospects for the inner retina. Eye (Lond.) *23*, 1980–1984.

19. Yu, S., Tanabe, T., Dezawa, M., Ishikawa, H., and Yoshimura, N. (2006). Effects of bone marrow stromal cell injection in an experimental glaucoma model. Biochem. Biophys. Res. Commun. *344*, 1071–1079.

20. Ding, S.L.S., Kumar, S., and Mok, P.L. (2017). Cellular reparative mechanisms of mesenchymal stem cells for retinal diseases. Int. J. Mol. Sci. *18*, E1406.

21. Johnson, T.V., DeKorver, N.W., Levasseur, V.A., Osborne, A., Tassoni, A., Lorber, B., Heller, J.P., Villasmil, R., Bull, N.D., Martin, K.R., and Tomarev, S.I. (2014). Identification of retinal ganglion cell neuroprotection conferred by platelet-derived growth factor through analysis of the mesenchymal stem cell secretome. Brain *137*, 503–519.

22. Taghi, G.M., Ghasem Kashani Maryam, H., Taghi, L., Leili, H., and Leyla, M. (2012). Characterization of in vitro cultured bone marrow and adipose tissue-derived mesenchymal stem cells and their ability to express neurotrophic factors. Cell Biol. Int. *36*, 1239–1249.

23. Sakai, K., Yamamoto, A., Matsubara, K., Nakamura, S., Naruse, M., Yamagata, M., Sakamoto, K., Tauchi, R., Wakao, N., Imagama, S., et al. (2012). Human dental pulp-derived stem cells promote locomotor recovery after complete transection of the rat spinal cord by multiple neuro-regenerative mechanisms. J. Clin. Invest. *122*, 80–90.

24. Wilkins, A., Kemp, K., Ginty, M., Hares, K., Mallam, E., and Scolding, N. (2009). Human bone marrow-derived mesenchymal stem cells secrete brain-derived neurotrophic factor which promotes neuronal survival in vitro. Stem Cell Res. (Amst.) *3*, 63–70.

25. Dormady, S.P., Bashayan, O., Dougherty, R., Zhang, X.M., and Basch, R.S. (2001). Immortalized multipotential mesenchymal cells and the hematopoietic microenvironment. J. Hematother. Stem Cell Res. *10*, 125–140.

26. Abumaree, M.H., Al Jumah, M.A., Kalionis, B., Jawdat, D., Al Khaldi, A., Abomaray, F.M., Fatani, A.S., Chamley, L.W., and Knawy, B.A. (2013). Human placental mesenchymal stem cells (pMSCs) play a role as immune suppressive cells by shifting macrophage differentiation from inflammatory M1 to anti-inflammatory M2 macrophages. Stem Cell Rev. Rep. *9*, 620–641.

27. Ribeiro, A., Laranjeira, P., Mendes, S., Velada, I., Leite, C., Andrade, P., Santos, F., Henriques, A., Grãos, M., Cardoso, C.M., et al. (2013). Mesenchymal stem cells from umbilical cord matrix, adipose tissue and bone marrow exhibit different capability to suppress peripheral blood B, natural killer and T cells. Stem Cell Res. Ther. *4*, 125.

28. Siqueira, R.C., Voltarelli, J.C., Messias, A.M.V., and Jorge, R. (2010). Possible mechanisms of retinal function recovery with the use of cell therapy with bone marrow-derived stem cells. Arq. Bras. Oftalmol. *73*, 474–479.

29. Oh, J.Y., Kim, M.K., Shin, M.S., Lee, H.J., Ko, J.H., Wee, W.R., and Lee, J.H. (2008). The anti-inflammatory and anti-angiogenic role of mesenchymal stem cells in corneal wound healing following chemical injury. Stem Cells *26*, 1047–1055.

30. Jiang, X.X., Zhang, Y., Liu, B., Zhang, S.X., Wu, Y., Yu, X.D., and Mao, N. (2005). Human mesenchymal stem cells inhibit differentiation and function of monocyte-derived dendritic cells. Blood *105*, 4120–4126.

31. Zhang, W., Ge, W., Li, C., You, S., Liao, L., Han, Q., Deng, W., and Zhao, R.C. (2004). Effects of mesenchymal stem cells on differentiation, maturation, and function of human monocyte-derived dendritic cells. Stem Cells Dev. *13*, 263–271.

32. Di Nicola, M., Carlo-Stella, C., Magni, M., Milanesi, M., Longoni, P.D., Matteucci, P., Grisanti, S., and Gianni, A.M. (2002). Human bone marrow stromal cells suppress T-lymphocyte proliferation induced by cellular or nonspecific mitogenic stimuli. Blood *99*, 3838–3843.

33. Gregory, C.A., Prockop, D.J., and Spees, J.L. (2005). Non-hematopoietic bone marrow stem cells: molecular control of expansion and differentiation. Exp. Cell Res. *306*, 330–335.

34. Dezawa, M., Kanno, H., Hoshino, M., Cho, H., Matsumoto, N., Itokazu, Y., Tajima, N., Yamada, H., Sawada, H., Ishikawa, H., et al. (2004). Specific induction of neuronal cells from bone marrow stromal cells and application for autologous transplantation. J. Clin. Invest. *113*, 1701–1710.

35. Kicic, A., Shen, W.Y., Wilson, A.S., Constable, I.J., Robertson, T., and Rakoczy, P.E. (2003). Differentiation of marrow stromal cells into photoreceptors in the rat eye. J. Neurosci. *23*, 7742–7749.

36. Beyer Nardi, N., and da Silva Meirelles, L. (2006). Mesenchymal stem cells: isolation, in vitro expansion and characterization. Handb. Exp. Pharmacol. (174), 249–282.

37. Ribeiro-Filho, A.C., Levy, D., Ruiz, J.L.M., Mantovani, M.D.C., and Bydlowski, S.P. (2019). Traditional and advanced cell cultures in hematopoietic stem cell studies. Cells *8*, E1628.

38. Sabel, B.A., Sautter, J., Stoehr, T., and Siliprandi, R. (1995). A behavioral model of excitotoxicity: retinal degeneration, loss of vision, and subsequent recovery after intraocular NMDA administration in adult rats. Exp. Brain Res. *106*, 93–105.

39. Lucas, D.R., and Newhouse, J.P. (1957). The toxic effect of sodium L-glutamate on the inner layers of the retina. AMA Arch. Opthalmol. *58*, 193–201.

40. Siliprandi, R., Canella, R., Carmignoto, G., Schiavo, N., Zanellato, A., Zanoni, R., and Vantini, G. (1992). *N*-methyl-D-aspartate-induced neurotoxicity in the adult rat retina. Vis. Neurosci. *8*, 567–573.

41. Sucher, N.J., Lipton, S.A., and Dreyer, E.B. (1997). Molecular basis of glutamate toxicity in retinal ganglion cells. Vision Res. *37*, 3483–3493.

42. Chang, B., Hawes, N.L., Hurd, R.E., Davisson, M.T., Nusinowitz, S., and Heckenlively, J.R. (2002). Retinal degeneration mutants in the mouse. Vision Res. *42*, 517–525.

43. Chang, B., Hawes, N.L., Pardue, M.T., German, A.M., Hurd, R.E., Davisson, M.T., Nusinowitz, S., Rengarajan, K., Boyd, A.P., Sidney, S.S., et al. (2007). Two mouse retinal degenerations caused by missense mutations in the beta-subunit of rod cGMP phosphodiesterase gene. Vision Res. *47*, 624–633.

44. Martínez-Fernández de la Cámara, C., Hernández-Pinto, A.M., Olivares-González, L., Cuevas-Martín, C., Sánchez-Aragó, M., Hervás, D., Salom, D., Cuezva, J.M., de la Rosa, E.J., Millán, J.M., and Rodrigo, R. (2015). Adalimumab reduces photoreceptor cell death in a mouse model of retinal degeneration. Sci. Rep. *5*, 11764.

45. Zlotnik, A., Yoshie, O., and Nomiyama, H. (2006). The chemokine and chemokine receptor superfamilies and their molecular evolution. Genome Biol. *7*, 243.

46. Zlotnik, A., and Yoshie, O. (2012). The chemokine superfamily revisited. Immunity *36*, 705–716.

47. Alexeev, V., Donahue, A., Uitto, J., and Igoucheva, O. (2016). Chemotaxis-driven disease-site targeting of therapeutic adult stem cells in dystrophic epidermolysis bullosa. Stem Cell Res. Ther. *7*, 124.

48. Shen, Z., Wang, J., Huang, Q., Shi, Y., Wei, Z., Zhang, X., Qiu, Y., Zhang, M., Wang, Y., Qin, W., et al. (2018). Genetic modification to induce CXCR2 overexpression in mesenchymal stem cells enhances treatment benefits in radiation-induced oral mucositis. Cell Death Dis. *9*, 229.

49. Chamberlain, G., Wright, K., Rot, A., Ashton, B., and Middleton, J. (2008). Murine mesenchymal stem cells exhibit a restricted repertoire of functional chemokine receptors: comparison with human. PLoS ONE *3*, e2934.

50. Dominici, M., Le Blanc, K., Mueller, I., Slaper-Cortenbach, I., Marini, F., Krause, D., Deans, R., Keating, A., Prockop, Dj., and Horwitz, E. (2006). Minimal criteria for defining multipotent mesenchymal stromal cells. The International Society for Cellular Therapy position statement. Cytotherapy *8*, 315–317.

51. Kohno, H., Sakai, T., and Kitahara, K. (2006). Induction of nestin, Ki-67, and cyclin D1 expression in Müller cells after laser injury in adult rat retina. Graefes Arch. Clin. Exp. Ophthalmol. *244*, 90–95.

52. Kolomeyer, A.M., and Zarbin, M.A. (2014). Trophic factors in the pathogenesis and therapy for retinal degenerative diseases. Surv. Ophthalmol. *59*, 134–165.

53. Labrador-Velandia, S., Alonso-Alonso, M.L., Di Lauro, S., García-Gutierrez, M.T., Srivastava, G.K., Pastor, J.C., and Fernandez-Bueno, I. (2019). Mesenchymal stem cells provide paracrine neuroprotective resources that delay degeneration of co-cultured organotypic neuroretinal cultures. Exp. Eye Res. *185*, 107671.

54. Hernández, R., Jiménez-Luna, C., Perales-Adán, J., Perazzoli, G., Melguizo, C., and Prados, J. (2020). Differentiation of human mesenchymal stem cells towards neuronal lineage: clinical trials in nervous system disorders. Biomol. Ther. (Seoul) *28*, 34–44.

55. Taran, R., Mamidi, M.K., Singh, G., Dutta, S., Parhar, I.S., John, J.P., Bhonde, R., Pal, R., and Das, A.K. (2014). In vitro and in vivo neurogenic potential of mesenchymal stem cells isolated from different sources. J. Biosci. *39*, 157–169.

56. Jiang, S.M., Zeng, L.P., Zeng, J.H., Tang, L., Chen, X.M., and Wei, X. (2015). β-III-tubulin: a reliable marker for retinal ganglion cell labeling in experimental models of glaucoma. Int. J. Ophthalmol. *8*, 643–652.

57. Jouhilahti, E.M., Peltonen, S., and Peltonen, J. (2008). Class III β-tubulin is a component of the mitotic spindle in multiple cell types. J. Histochem. Cytochem. *56*, 1113–1119.

58. Prigent, C., and Dimitrov, S. (2003). Phosphorylation of serine 10 in histone H3, what for? J. Cell Sci. *116*, 3677–3685.

59. Levkovitch-Verbin, H., Sadan, O., Vander, S., Rosner, M., Barhum, Y., Melamed, E., Offen, D., and Melamed, S. (2010). Intravitreal injections of neurotrophic factors secreting mesenchymal stem cells are neuroprotective in rat eyes following optic nerve transection. Invest. Ophthalmol. Vis. Sci. *51*, 6394–6400.

60. Singer, N.G., and Caplan, A.I. (2011). Mesenchymal stem cells: mechanisms of inflammation. Annu. Rev. Pathol. *6*, 457–478.

61. Baglio, S.R., Pegtel, D.M., and Baldini, N. (2012). Mesenchymal stem cell secreted vesicles provide novel opportunities in (stem) cell-free therapy. Front. Physiol. *3*, 359.

62. Zhang, Y., and Wang, W. (2010). Effects of bone marrow mesenchymal stem cell transplantation on light-damaged retina. Invest. Ophthalmol. Vis. Sci. *51*, 3742–3748.

63. Tzameret, A., Sher, I., Belkin, M., Treves, A.J., Meir, A., Nagler, A., Levkovitch-Verbin, H., Rotenstreich, Y., and Solomon, A.S. (2015). Epiretinal transplantation of human bone marrow mesenchymal stem cells rescues retinal and vision function in a rat model of retinal degeneration. Stem Cell Res. (Amst.) *15*, 387–394.

64. Keshtkar, S., Azarpira, N., and Ghahremani, M.H. (2018). Mesenchymal stem cell-derived extracellular vesicles: novel frontiers in regenerative medicine. Stem Cell Res. Ther. *9*, 63.

65. Tsiapalis, D., and O'Driscoll, L. (2020). Mesenchymal stem cell derived extracellular vesicles for tissue engineering and regenerative medicine applications. Cells *9*, E991.

66. Furuta, T., Miyaki, S., Ishitobi, H., Ogura, T., Kato, Y., Kamei, N., Miyado, K., Higashi, Y., and Ochi, M. (2016). Mesenchymal stem cell-derived exosomes promote fracture healing in a mouse model. Stem Cells Transl. Med. *5*, 1620–1630.

67. Zhang, S., Chuah, S.J., Lai, R.C., Hui, J.H.P., Lim, S.K., and Toh, W.S. (2018). MSC exosomes mediate cartilage repair by enhancing proliferation, attenuating apoptosis and modulating immune reactivity. Biomaterials *156*, 16–27.

68. Reza-Zaldivar, E.E., Hernández-Sapiéns, M.A., Gutiérrez-Mercado, Y.K., Sandoval-Ávila, S., Gomez-Pinedo, U., Márquez-Aguirre, A.L., Vázquez-Méndez, E., Padilla-Camberos, E., and Canales-Aguirre, A.A. (2019). Mesenchymal stem cell-derived exosomes promote neurogenesis and cognitive function recovery in a mouse model of Alzheimer's disease. Neural Regen. Res. *14*, 1626–1634.

69. Li, C., Jiao, G., Wu, W., Wang, H., Ren, S., Zhang, L., Zhou, H., Liu, H., and Chen, Y. (2019). Exosomes from bone marrow mesenchymal stem cells inhibit neuronal apoptosis and promote motor function recovery via the Wnt/β-catenin signaling pathway. Cell Transplant. *28*, 1373–1383.

70. Lu, Y., Zhou, Y., Zhang, R., Wen, L., Wu, K., Li, Y., Yao, Y., Duan, R., and Jia, Y. (2019). Bone mesenchymal stem cell-derived extracellular vesicles promote recovery following spinal cord injury via improvement of the integrity of the blood-spinal cord barrier. Front. Neurosci. *13*, 209.

71. Doeppner, T.R., Herz, J., Görgens, A., Schlechter, J., Ludwig, A.K., Radtke, S., de Miroschedji, K., Horn, P.A., Giebel, B., and Hermann, D.M. (2015). Extracellular vesicles improve post-stroke neuroregeneration and prevent postischemic immunosuppression. Stem Cells Transl. Med. *4*, 1131–1143.

72. Clark, K., Zhang, S., Barthe, S., Kumar, P., Pivetti, C., Kreutzberg, N., Reed, C., Wang, Y., Paxton, Z., Farmer, D., et al. (2019). Placental mesenchymal stem cell-derived extracellular vesicles promote myelin regeneration in an animal model of multiple sclerosis. Cells *8*, E1497.

73. Haga, H., Yan, I.K., Takahashi, K., Matsuda, A., and Patel, T. (2017). Extracellular vesicles from bone marrow-derived mesenchymal stem cells improve survival from lethal hepatic failure in mice. Stem Cells Transl. Med. *6*, 1262–1272.

74. Li, T., Yan, Y., Wang, B., Qian, H., Zhang, X., Shen, L., Wang, M., Zhou, Y., Zhu, W., Li, W., and Xu, W. (2013). Exosomes derived from human umbilical cord mesenchymal stem cells alleviate liver fibrosis. Stem Cells Dev. *22*, 845–854.

75. Mardpour, S., Ghanian, M.H., Sadeghi-Abandansari, H., Mardpour, S., Nazari, A., Shekari, F., and Baharvand, H. (2019). Hydrogel-mediated sustained systemic delivery of mesenchymal stem cell-derived extracellular vesicles improves hepatic regeneration in chronic liver failure. ACS Appl. Mater. Interfaces *11*, 37421–37433.

76. Matsukura, T., Inaba, C., Weygant, E.A., Kitamura, D., Janknecht, R., Matsumoto, H., Hyink, D.P., Kashiwada, S., and Obara, T. (2019). Extracellular vesicles from human bone marrow mesenchymal stem cells repair organ damage caused by cadmium poisoning in a medaka model. Physiol. Rep. *7*, e14172.

77. He, J., Wang, Y., Sun, S., Yu, M., Wang, C., Pei, X., Zhu, B., Wu, J., and Zhao, W. (2012). Bone marrow stem cells-derived microvesicles protect against renal injury in the mouse remnant kidney model. Nephrology (Carlton) *17*, 493–500.

78. Nakamura, Y., Miyaki, S., Ishitobi, H., Matsuyama, S., Nakasa, T., Kamei, N., Akimoto, T., Higashi, Y., and Ochi, M. (2015). Mesenchymal-stem-cell-derived exosomes accelerate skeletal muscle regeneration. FEBS Lett. *589*, 1257–1265.

79. Mitchell, R., Mellows, B., Sheard, J., Antonioli, M., Kretz, O., Chambers, D., Zeuner, M.T., Tomkins, J.E., Denecke, B., Musante, L., et al. (2019). Secretome of adipose-derived mesenchymal stem cells promotes skeletal muscle regeneration through synergistic action of extracellular vesicle cargo and soluble proteins. Stem Cell Res. Ther. *10*, 116.

80. Lai, R.C., Arslan, F., Lee, M.M., Sze, N.S., Choo, A., Chen, T.S., Salto-Tellez, M., Timmers, L., Lee, C.N., El Oakley, R.M., et al. (2010). Exosome secreted by MSC reduces myocardial ischemia/reperfusion injury. Stem Cell Res. (Amst.) *4*, 214–222.

81. Huang, P., Wang, L., Li, Q., Xu, J., Xu, J., Xiong, Y., Chen, G., Qian, H., Jin, C., Yu, Y., et al. (2019). Combinatorial treatment of acute myocardial infarction using stem cells and their derived exosomes resulted in improved heart performance. Stem Cell Res. Ther. *10*, 300.

82. Mathew, B., Ravindran, S., Liu, X., Torres, L., Chennakesavalu, M., Huang, C.C., Feng, L., Zelka, R., Lopez, J., Sharma, M., and Roth, S. (2019). Mesenchymal stem cell-derived extracellular vesicles and retinal ischemia-reperfusion. Biomaterials *197*, 146–160.

83. Mead, B., Ahmed, Z., and Tomarev, S. (2018). Mesenchymal stem cell-derived small extracellular vesicles promote neuroprotection in a genetic DBA/2J mouse model of glaucoma. Invest. Ophthalmol. Vis. Sci. *59*, 5473–5480.

84. Shigemoto-Kuroda, T., Oh, J.Y., Kim, D.K., Jeong, H.J., Park, S.Y., Lee, H.J., Park, J.W., Kim, T.W., An, S.Y., Prockop, D.J., and Lee, R.H. (2017). MSC-derived extracellular vesicles attenuate immune responses in two autoimmune murine models: type 1 diabetes and uveoretinitis. Stem Cell Reports *8*, 1214–1225.

85. Guzman, R., Janowski, M., and Walczak, P. (2018). Intra-arterial delivery of cell therapies for stroke. Stroke *49*, 1075–1082.

86. Huang, J., Zhang, Z., Guo, J., Ni, A., Deb, A., Zhang, L., Mirotsou, M., Pratt, R.E., and Dzau, V.J. (2010). Genetic modification of mesenchymal stem cells overexpressing CCR1 increases cell viability, migration, engraftment, and capillary density in the injured myocardium. Circ. Res. *106*, 1753–1762.

87. Alexeev, V., Donahue, A., Uitto, J., and Igoucheva, O. (2013). Analysis of chemotactic molecules in bone marrow-derived mesenchymal stem cells and the skin: Ccl27-Ccr10 axis as a basis for targeting to cutaneous tissues. Cytotherapy *15*, 171–184.e1.

88. Proudfoot, A.E., and Uguccioni, M. (2016). Modulation of chemokine responses: synergy and cooperativity. Front. Immunol. *7*, 183.

89. Mellado, M., Rodríguez-Frade, J.M., Vila-Coro, A.J., Fernández, S., Martín de Ana, A., Jones, D.R., Torán, J.L., and Martínez-A, C. (2001). Chemokine receptor homo- or heterodimerization activates distinct signaling pathways. EMBO J. *20*, 2497–2507.

90. Gouwy, M., Struyf, S., Noppen, S., Schutyser, E., Springael, J.Y., Parmentier, M., Proost, P., and Van Damme, J. (2008). Synergy between coproduced CC and CXC chemokines in monocyte chemotaxis through receptor-mediated events. Mol. Pharmacol. *74*, 485–495.

91. Nagineni, C.N., Kommineni, V.K., Ganjbaksh, N., Nagineni, K.K., Hooks, J.J., and Detrick, B. (2015). Inflammatory cytokines induce expression of chemokines by human retinal cells: role in chemokine receptor mediated age-related macular degeneration. Aging Dis. *6*, 444–455.

92. Crane, I.J., and Liversidge, J. (2008). Mechanisms of leukocyte migration across the blood-retina barrier. Semin. Immunopathol. *30*, 165–177.

93. Crane, I.J., Wallace, C.A., McKillop-Smith, S., and Forrester, J.V. (2000). Control of chemokine production at the blood-retina barrier. Immunology *101*, 426–433.

94. Uren, P.J., Lee, J.T., Doroudchi, M.M., Smith, A.D., and Horsager, A. (2014). A profile of transcriptomic changes in the *rd10* mouse model of retinitis pigmentosa. Mol. Vis. *20*, 1612–1628.

95. Crane, I.J., Xu, H., Wallace, C., Manivannan, A., Mack, M., Liversidge, J., Marquez, G., Sharp, P.F., and Forrester, J.V. (2006). Involvement of CCR5 in the passage of Th1-type cells across the blood-retina barrier in experimental autoimmune uveitis. J. Leukoc. Biol. *79*, 435–443.

96. Crane, I.J., McKillop-Smith, S., Wallace, C.A., Lamont, G.R., and Forrester, J.V. (2001). Expression of the chemokines MIP-1α, MCP-1, and RANTES in experimental autoimmune uveitis. Invest. Ophthalmol. Vis. Sci. *42*, 1547–1552.

97. Foxman, E.F., Zhang, M., Hurst, S.D., Muchamuel, T., Shen, D., Wawrousek, E.F., Chan, C.C., and Gery, I. (2002). Inflammatory mediators in uveitis: differential induction of cytokines and chemokines in Th1- versus Th2-mediated ocular inflammation. J. Immunol. *168*, 2483–2492.

98. Rutar, M., Natoli, R., Chia, R.X., Valter, K., and Provis, J.M. (2015). Chemokine-mediated inflammation in the degenerating retina is coordinated by Müller cells, activated microglia, and retinal pigment epithelium. J. Neuroinflammation *12*, 8.

99. Zeng, H., Lai, H., Lai, S., and Tso, M.O. (2006). Localization of chemokines and chemokine receptors in the retina of RD mice. Invest. Ophthalmol. Vis. Sci. *47*, 5772.

100. Andrzejewska, A., Dabrowska, S., Nowak, B., Walczak, P., Lukomska, B., and Janowski, M. (2020). Mesenchymal stem cells injected into carotid artery to target focal brain injury home to perivascular space. Theranostics *10*, 6615–6628.

101. Assis, A.C.M., Carvalho, J.L., Jacoby, B.A., Ferreira, R.L., Castanheira, P., Diniz, S.O., Cardoso, V.N., Goes, A.M., and Ferreira, A.J. (2010). Time-dependent migration of systemically delivered bone marrow mesenchymal stem cells to the infarcted heart. Cell Transplant. *19*, 219–230.

102. Barbash, I.M., Chouraqui, P., Baron, J., Feinberg, M.S., Etzion, S., Tessone, A., Miller, L., Guetta, E., Zipori, D., Kedes, L.H., et al. (2003). Systemic delivery of bone marrow-derived mesenchymal stem cells to the infarcted myocardium: feasibility, cell migration, and body distribution. Circulation *108*, 863–868.

103. Kraitchman, D.L., Tatsumi, M., Gilson, W.D., Ishimori, T., Kedziorek, D., Walczak, P., Segars, W.P., Chen, H.H., Fritzges, D., Izbudak, I., et al. (2005). Dynamic imaging of allogeneic mesenchymal stem cells trafficking to myocardial infarction. Circulation *112*, 1451–1461.

104. Eggenhofer, E., Benseler, V., Kroemer, A., Popp, F.C., Geissler, E.K., Schlitt, H.J., Baan, C.C., Dahlke, M.H., and Hoogduijn, M.J. (2012). Mesenchymal stem cells are short-lived and do not migrate beyond the lungs after intravenous infusion. Front. Immunol. *3*, 297.

105. Boulland, J.L., Leung, D.S., Thuen, M., Vik-Mo, E., Joel, M., Perreault, M.C., Langmoen, I.A., Haraldseth, O., and Glover, J.C. (2012). Evaluation of intracellular labeling with micron-sized particles of iron oxide (MPIOs) as a general tool for in vitro and in vivo tracking of human stem and progenitor cells. Cell Transplant. *21*, 1743–1759.

106. Qiu, G., Seiler, M.J., Mui, C., Arai, S., Aramant, R.B., de Juan, E., Jr., and Sadda, S. (2005). Photoreceptor differentiation and integration of retinal progenitor cells transplanted into transgenic rats. Exp. Eye Res. *80*, 515–525.

107. Coles, B.L.K., Angénieux, B., Inoue, T., Del Rio-Tsonis, K., Spence, J.R., McInnes, R.R., Arsenijevic, Y., and van der Kooy, D. (2004). Facile isolation and the characterization of human retinal stem cells. Proc. Natl. Acad. Sci. USA *101*, 15772–15777.

108. Klassen, H.J., Ng, T.F., Kurimoto, Y., Kirov, I., Shatos, M., Coffey, P., and Young, M.J. (2004). Multipotent retinal progenitors express developmental markers, differentiate into retinal neurons, and preserve light-mediated behavior. Invest. Ophthalmol. Vis. Sci. *45*, 4167–4173.

109. Chacko, D.M., Rogers, J.A., Turner, J.E., and Ahmad, I. (2000). Survival and differentiation of cultured retinal progenitors transplanted in the subretinal space of the rat. Biochem. Biophys. Res. Commun. *268*, 842–846.

110. Yoshimura, T., Sonoda, K.H., Sugahara, M., Mochizuki, Y., Enaida, H., Oshima, Y., Ueno, A., Hata, Y., Yoshida, H., and Ishibashi, T. (2009). Comprehensive analysis of inflammatory immune mediators in vitreoretinal diseases. PLoS ONE *4*, e8158.

111. Roh, M.I., Kim, H.S., Song, J.H., Lim, J.B., and Kwon, O.W. (2009). Effect of intravitreal bevacizumab injection on aqueous humor cytokine levels in clinically significant macular edema. Ophthalmology *116*, 80–86.

112. Funatsu, H., Yamashita, H., Noma, H., Mimura, T., Nakamura, S., Sakata, K., and Hori, S. (2005). Aqueous humor levels of cytokines are related to vitreous levels

and progression of diabetic retinopathy in diabetic patients. Graefes Arch. Clin. Exp. Ophthalmol. *243*, 3–8.

113. Liu, F., Ding, X., Yang, Y., Li, J., Tang, M., Yuan, M., Hu, A., Zhan, Z., Li, Z., and Lu, L. (2016). Aqueous humor cytokine profiling in patients with wet AMD. Mol. Vis. *22*, 352–361.

114. Yoshida, N., Ikeda, Y., Notomi, S., Ishikawa, K., Murakami, Y., Hisatomi, T., Enaida, H., and Ishibashi, T. (2013). Clinical evidence of sustained chronic inflammatory reaction in retinitis pigmentosa. Ophthalmology *120*, 100–105.

115. Hardee, C.L., Arévalo-Soliz, L.M., Hornstein, B.D., and Zechiedrich, L. (2017). Advances in Non-Viral DNA Vectors for Gene Therapy. Genes (Basel) *8*, E65.

116. Kilkenny, C., Browne, W., Cuthill, I.C., Emerson, M., and Altman, D.G.; National Centre for the Replacement, Refinement and Reduction of Amimals in Research (2011). Animal research: reporting in vivo experiments–the ARRIVE guidelines. J. Cereb. Blood Flow Metab. *31*, 991–993.

117. Liang, F.Q., Anand, V., Maguire, A.M., and Bennett, J. (2001). Intraocular delivery of recombinant virus. Methods Mol. Med. *47*, 125–139.